Plant Stress 18 (2025) 101115

Contents lists available at ScienceDirect

Plant Stress

journal homepage: www.sciencedirect.com/journal/plant-stress

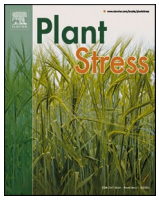

Integrative morpho-physiological and transcriptomic insights into wheat responses to combined drought, heat, and elevated CO_2 under future climate conditions

Zbyněk Milec [a,1], Kashif Nawaz [b,1], Swati Puranik [a,c], Anna Nowicka [d], Martin Kovačik [d], Hana Findurová [a], Emmanuel Opoku [a], Ales Pecinka [d], Karel Klem [a], Otmar Urban [a], Pranav Pankaj Sahu [a,*]

[a] Global Change Research Institute of the Czech Academy of Sciences, Bělidla 986/4a, 603 00 Brno, Czech Republic
[b] Biological and Environmental Science and Engineering (BESE), King Abdullah University of Science and Technology (KAUST), Saudi Arabia
[c] Rothamsted Research, West Common, Harpenden, AL5 2JQ, UK
[d] Institute of Experimental Botany of the Czech Academy of Sciences, Centre of Plant Structural and Functional Genomics, Šlechtitelů 31, 779 00 Olomouc, Czech Republic

ARTICLE INFO

Keywords:
Climate change
Wheat
Drought
Elevated CO_2
Elevated temperature
Morpho-physiology
Transcriptome analysis

ABSTRACT

Climate change intensifies environmental stressors such as drought and heat, posing a significant threat to crop productivity, while elevated CO_2 concentrations generally have a positive effect on photosynthetic performance and, under certain conditions, can compensate for the negative effects of stress factors. We investigated the morpho-physiological and transcriptional responses of bread wheat (*Triticum aestivum* L.) to drought (D), elevated temperature (eT), and elevated CO_2 (eC) applied individually, in pairs (eT+D, eC+D, eC+eT), and as a triple combination (eC+eT+D). The eT+D combination resulted in the most severe reductions in growth and yield, whereas eC consistently enhanced water-use efficiency. Transcriptome profiling revealed extensive reprogramming of gene expression under multifactorial treatment, including enrichment of hormone signalling and photosynthesis pathways. Key transcription factor families (e.g., MYB, NAC, WRKY) and potential marker genes were differentially regulated across treatments. Co-expression network analysis identified gene modules associated with critical traits, such as shoot biomass and grain yield, emphasising roles for stress-responsive signalling. These findings advance our understanding of wheat adaptation to climate-related stress combinations and provide molecular targets for breeding climate-resilient cultivars.

Introduction

Bread wheat (*Triticum aestivum* L.), an allohexaploid with AABBDD subgenomes (Ramírez-González et al., 2018), is a staple cereal crop that is essential for global food security (Shiferaw et al., 2013). However, climate change is intensifying abiotic stressors – such as drought and elevated temperatures – that could threaten wheat productivity. These factors may interact in complex ways, resulting in synergistic, additive, or antagonistic effects (Sato et al., 2024). While the impacts of individual stressors are relatively well understood (Shah et al., 1999; Tahmasebi et al., 2017; Prasad et al., 2011; Tricker et al., 2018), their combined effects remain poorly characterised, which hinders breeding efforts aimed at enhancing resilience.

Global climate models predict that atmospheric CO_2 concentrations will exceed 700 ppm by the end of the century, accompanied by average temperature increases of 2 °C to 4 °C (Intergovernmental Panel on Climate Change 2015). These changes are expected to increase the frequency of extreme weather events, including prolonged heatwaves and severe droughts (Tripathy et al., 2023), particularly in the key wheat-producing regions such as Southern and Central Europe and the Mediterranean basin (Lorite et al., 2023). Overall, these climatic trends are projected to reduce wheat yields, resulting in significant socio-economic consequences for a growing global population (Holman et al., 2021).

* Corresponding author.
E-mail address: sahu.p@czechglobe.cz (P.P. Sahu).
[1] These authors contributed equally to this work.

https://doi.org/10.1016/j.stress.2025.101115
Received 15 July 2025; Received in revised form 9 October 2025; Accepted 1 November 2025
Available online 3 November 2025

By 2050, the global population is projected to increase by approximately 2 billion people – rising from about 7.7 billion in 2020 to roughly 9.7 billion – significantly raising the demand for food production. In particular, projections indicate that an additional 132 million metric tonnes of wheat will be required annually, assuming constant *per capita* consumption (Erenstein et al., 2022). This highlights the urgency of addressing the negative impacts of drought and heat, two major constraints on wheat productivity (Cohen et al., 2021). Drought limits soil water availability, reducing stomatal conductance and altering resource reallocation, while heat stress further impairs photosynthesis (Onyemaobi et al., 2021; Rizhsky et al., 2002; Bita and Gerats, 2013). In contrast, elevated CO_2 can partially mitigate these effects by enhancing photosynthetic efficiency and improving water-use efficiency (Shanmugam et al., 2013; Abdelhakim et al., 2021). However, the combined effects of elevated CO_2 with drought and heat often result in non-additive and unpredictable outcomes that deviate from predictions based on single-stressor studies, emphasizing the need for multifactorial investigations.

The plant́s response to environmental stressors involves intricate molecular processes that activate or suppress numerous metabolic pathways (Bita and Gerats, 2013). However, transcriptomic studies in cereals remain limited and are often restricted to single or dual-stress conditions, such as heat or heat combined with drought, and typically focus on early growth phases or specific developmental stages such as flowering (Liu et al., 2015; Azameti et al., 2022; Qin et al., 2008; Ma et al., 2017). Furthermore, although elevated CO_2 is increasingly recognised as an important modulator of plant stress responses, few studies in temperate cereals have examined its interactive effects with heat stress (Vicente et al., 2019; Lin et al., 2016). These research gaps emphasize the need for comprehensive transcriptomic studies that address multiple stressors to enhance our understanding of the genetic networks underlying stress tolerance in cereals.

At the molecular level, co-occurring drought, heat, and elevated CO_2 trigger early Ca^{2+}/ROS signatures and ABA-centred cross-talk that converge on MAPK and SnRK2/OST1 hubs to reshape transcription and primary metabolism (Ravi et al., 2023). Exposure to multiple factors commonly produces non-additive responses, rather than additive single-factor effects (Zandalinas and Mittler, 2022). Heat activates an HSFA1–HSP proteostasis program and wider TF networks (HSFs, NAC, WRKY, ERF/bZIP), stabilizing proteins while reprioritizing growth (Kan et al., 2023; Ohama et al., 2017). Stomatal and hydraulic control couple upstream signals to gas exchange: ABA/SnRK2 activity tunes guard-cell ion transport in real time, and aquaporins such as *PIP2;1* facilitate H_2O_2 influx that amplifies stomatal closure (Zhang et al., 2020; Rodrigues et al., 2017). Elevated CO_2 adds another regulatory layer by shifting redox/hormone set points and improving water-use efficiency; in wheat, elevated CO_2 can partly buffer heat injury to photosynthesis, yet interactions with drought/heat remain context-dependent (Chavan et al., 2019). These pathway-level insights motivate an integrative, multifactorial transcriptome–phenotype analysis in wheat.

In this study, we address critical knowledge gaps by examining wheat responses to individual and combined stress conditions under current and future CO_2 concentrations. Specifically, we investigated the effects of drought (D), elevated temperature (eT), and elevated CO_2 (eC), as well as their combinations (eT+D, eC+D, eC+eT, and eC+eT+D). Through an integrated approach that encompasses morphological, physiological, and transcriptomic analyses, we aimed to elucidate: how wheat orchestrates its morpho-physiological and molecular networks to navigate complex, multifactorial stress environments; how drought and elevated temperature – applied individually or in combination – affect key morphological, physiological, and yield-related traits in wheat, and to what extent elevated CO_2 can mitigate these effects in various types of interactions. Our findings may inform breeding programmes and agronomic strategies, ensuring sustainable wheat production in the face of rapidly changing global climates.

Materials and methods

Plant materials and initial growth conditions

The winter bread wheat cultivar Alana (*Triticum aestivum* L. subsp. *aestivum*, Accession No. 01C0106569) was obtained from the Research Institute of Crop Production in Prague, Czech Republic. Seeds were imbibed in Petri dishes lined with moistened cellulose paper, stratified at 4 °C in the dark for 24 h, and then germinated in the dark at 25 °C for three days. Following germination, seedlings were transplanted into pots (11 × 11 × 25 cm) filled with a Klasmann TS2 substrate and sand mixture (2:1, v/v) (Klasmann-Deilmann, Geeste, Germany). Plants were grown in a FytoScope FS-SI 3400 growth chamber (PSI, Drásov, Czech Republic) under an 11 h light/13 h dark photoperiod, with day/night temperatures of 20 °C/16 °C, and 60 % relative air humidity (RH) for 10 days. Subsequently, the plants were vernalized for 8 weeks at 6 °C under short-day conditions (8 h light/16 h dark, 85 % RH). After vernalization, they were grown under long-day conditions (15 h light/9 h dark, 14 °C/8 °C, 60 % RH, 200 μmol m^{-2} s^{-1}) until 85 days after germination when stress treatments commenced (Fig. 1).

Experimental setup based on IPCC climate projections

Experiments were designed to simulate both current and projected future climate conditions for Brno, Czech Republic (49.19° N, 16.60° E), a region with a temperate continental climate. Climate data were collected for two distinct periods: a recent baseline (1991–2020; hereinafter referred to as control or Ctr) and a future projection (2080–2099; hereinafter referred to as 2100), based on the Representative Concentration Pathway 8.5 (RCP 8.5) scenario (https://tntcat.iiasa.ac.at/RcpDb).

Current and projected diurnal temperature profiles, along with monthly maximum (T_{max}) and minimum (T_{min}) temperatures, were obtained from the World Bank's Climate Change Knowledge Portal (https://climateknowledgeportal.worldbank.org/, accessed March 2020; Table S1). Control plants were grown under a temperature regime that simulated natural diurnal variation, with the following monthly day/night profiles: May – 20°/8 °C; June – 23 °C/12 °C; and July – 25 °C/13 °C (Table S1). Plants were maintained at 400 ppm CO_2 and 90 ± 5 % soil water capacity (SWC).

To simulate future environmental conditions, seven distinct treatments were applied: three single-factor treatments – drought (D), elevated temperature (eT), and elevated CO_2 concentration (eC); three two-factor combinations – eT+D, eC+D, and eC+eT; and one three-factor combination – eC+eT+D. The elevated temperature (eT) regime was based on projected average conditions for year 2100 and involved increasing day/night temperatures to: May – 23 °C/12 °C; June – 28 °C/16 °C; and July – 31 °C/19 °C (Table S1). Drought (D) was imposed by reducing SWC to 25 ± 5 %, simulating moderate drought conditions. SWC was monitored gravimetrically three times per week and adjusted as necessary to maintain consistent levels throughout the experiment. Elevated CO_2 (eC) was set at 700 ppm, reflecting atmospheric CO_2 concentrations projected for the end of the century (Fig. 1A).

Photoperiod was adjusted to match the natural day lengths of May, June and July; RH was held at 65 % during the light period and 90 % in the dark. Light intensity was likewise tuned to the monthly profile, peaking at 800 ± 50 μmol m^{-2} s^{-1}. Plants were monitored daily, and environmental parameters were continuously recorded to ensure precision and consistency across all treatments. The experimental treatments (drought, elevated temperature, and elevated CO_2) commenced at the onset of stem elongation (GS30) and continued until seed development (GS70), both critical stages in wheat growth. After the treatments, all plants were transferred back to control conditions (Fig. 1B).

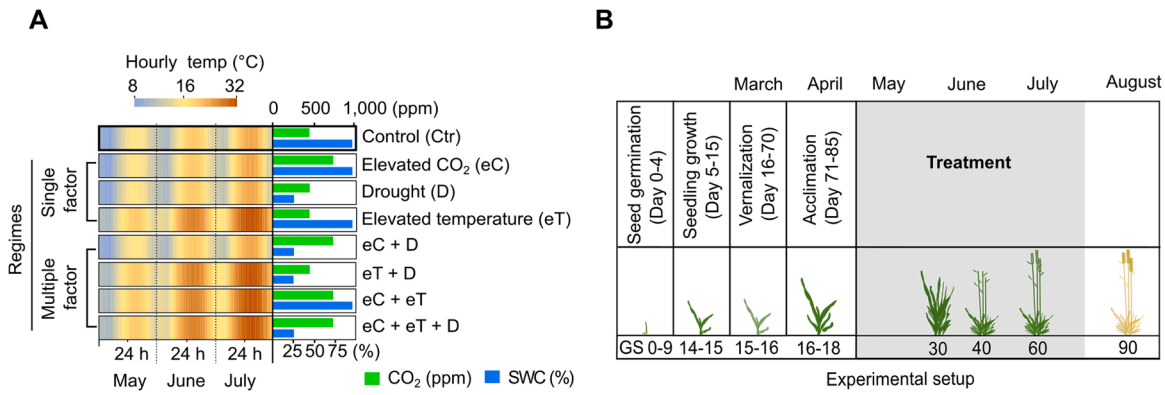

Fig. 1. Overview of treatment regimes applied to bread wheat (*T. aestivum* L.) under current (2020) and projected future (2100) temperate-continental climate scenarios with elevated atmospheric CO_2.
The experimental setup simulated the effects of water availability, temperature, and atmospheric CO_2 concentration and their combinations under environmental conditions representative of Central Europe (Brno, Czech Republic). (A) Climate regimes. The left panel shows hourly temperature profiles under each treatment. Control conditions reflected current climate averages, with daily temperature ranges of 8/20 °C (May), 12/23 °C (June), and 13/25 °C (July). In future-like treatments, temperatures were increased to 12/23 °C (May), 16/28 °C (June), and 19/31 °C (July). Temperature varied gradually over 24 h to mimic natural diurnal cycles and was maintained from May to July, aligning with critical wheat growth stages. The right panel illustrates soil water capacity (SWC) and atmospheric CO_2 concentrations used in each treatment. Control plants were maintained at 90 % SWC and 400 ppm CO_2. In future scenarios, drought reduced SWC to 25 ± 5 %, while CO_2 concentration (eC) was elevated to 700 ppm. Treatments included drought (D) and elevated temperature (eT) as stressors, and elevated CO_2 concentration (eC) as a potential stress-mitigating factor. These were applied individually, in all pairwise combinations (eT+D, eC+D, and eC+eT), and as a three-factor combination (eC+eT+D). (B) Experimental setup. The timeline shows the growth conditions prior to and during the treatment period, aligned with key developmental stages of winter wheat, based on the Zadoks growth scale (GS). Treatments were applied from stem elongation (GS30) through the completion of anthesis (GS69). After treatments, all plants were returned to control regime.

Measurement of plant morphological parameters

Morphological traits were assessed at the ripening stage (GS91) using three replicates per treatment regime, each comprising six plants. An exception was made for flag leaf length (FLL), which was measured earlier, at the flowering stage (GS61). Plant height (PH) was measured from the soil surface to the tip of the central spike. FLL was measured from the base to the tip of the flag leaf on the main stem. Shoot biomass (SBM) was obtained by cutting the shoots at the soil surface, oven-drying them at 70 °C for 48 h and then weighing. The number of spikes per plant (NoSP) was counted manually. Spike biomass (SPBM) was determined by separating the spikes, drying them under the same conditions as SBM, and weighing. Spike length (SPL) was recorded from the base to the tip of the central spike. Husk weight (HUWt) was measured after the husks were separated from the grains and dried using the same procedure as for SBM.

Measurement of grain morphological parameters

Grains were collected at the seed dormancy stage. After harvest, the threshed grains were stored at room temperature for one month prior to analysis. All analyses were conducted using three biological replicates per treatment regime, each consisting of grains collected from six plants. The total number of grains per plant (NoG) was counted using the *SeedExtractor* tool (Zhu et al., 2021). Thousand grain weight (TGW) was calculated by weighing 150 randomly selected grains per plant, with TGW determined as (total sample weight [g] / number of grains) × 1000. Grain dimensions, including area (AR), length (GL), width (GW), and periphery (PER), were determined using the *SeedExtractor* tool (Zhu et al., 2021) on approximately 150 grains per plant. Periphery was defined as the external boundary length of each grain. Grain circularity (CIR) was calculated as $4\pi \times AR / PER^2$, and the width-to-length ratio (GW/GL) was determined by dividing grain width by grain length.

Measurement of physiological parameters

Physiological traits, including transpiration rate (E), photosynthetic rate (A), stomatal conductance (G_{SW}), and intrinsic water-use efficiency (WUE), were measured at the flowering stage (GS61) using three replicates per stress regime, each consisting of six plants. Measurements were taken from the second and third fully expanded intact leaves of the main tiller, 5–8 h after the beginning of the light period, using a Li-6400 portable photosynthesis system (LI-COR Biosciences, Lincoln, Nebraska, USA). Intrinsic WUE was calculated as the ratio of A to E (WUE = A/E).

Stomata status assessment

Stomatal imprinting was conducted on three representative plants for each treatment, with a minimum of 500 stomatal cells evaluated per plant for each regime, following the method described in (He et al., 2019). Briefly, Silagum-Light (DMG, Germany) was prepared by mixing its base and catalyst in a 1:1 ratio and applied to the abaxial surface of the leaf. Once the material hardened, the negative mold was carefully removed. A thin layer of nail polish was then applied to this mold, allowed to dry, and subsequently peeled off to create a positive imprint. This imprint was transferred to a glass slide immersed in 50 % glycerol. Images were captured using a light microscope (Olympus BX60) equipped with a Promicra 3–3CP camera (Sony). The status was categorised as open, partially open, or closed.

RNA extraction, sequencing and data analysis

Leaf samples (3 cm from the mid-section of the third and fourth leaves on the main tiller) were collected from three biological replicates per treatment at GS61. Total RNA was extracted using the RNeasy Plant Mini Kit (Qiagen), including an on-column DNase I treatment. RNA integrity (RIN > 6.0) was verified using a Bioanalyzer 2100 (Agilent). Libraries were prepared (NEBNext Ultra RNA Library Prep Kit for Illumina, poly-A enrichment) and sequenced on an Illumina NovaSeq 6000 (150 bp paired-end, Novogene Ltd, UK). Raw sequencing reads were processed using Trim Galore v.0.4.1 to remove adaptor sequences and low-quality bases. Cleaned reads were subsequently aligned to the wheat reference genome (RefSeq v2.0, EnsemblPlants) using HISAT2 (Kim et al., 2019). The evaluation table of RNA sequence data quality is provided in the Table S2. Differential gene expression analyses were performed with DESeq2 (Love et al., 2014), considering genes with an

FDR-adjusted p-value < 0.05 as significantly differentially expressed. Expression levels were reported in fragments per kilobase of transcript per million mapped reads (FPKM). Multidimensional scaling (MDS) was performed post-variance stabilization, with data visualisation (Volcano and UpSet plots) conducted using R's ggplot2 package. Gene ontology (GO) enrichment analysis of biological processes and KEGG pathways was carried out in ShinyGO 0.85 (http://bioinformatics.sdstate.edu/go/) using a triad-collapsed list of differentially expressed genes (DEGs), in which one representative gene was retained per homoeologous triad to avoid overcounting A/B/D copies. DEGs were defined by an adjusted p-value < 0.01 and an absolute log2-fold change ($\log_2$FC) ≥ 1. Enrichment analysis applied an FDR cutoff of 0.05 and a minimum pathway size of 10 genes, followed by the removal of redundant terms. The list of triads was retrieved from Wang et al. (Wang et al., 2025). Functional annotations of all genes were conducted using DAVID bioinformatics resources (https://davidbioinformatics.nih.gov/tools.jsp) (Sherman et al., 2022; Huang et al., 2009). Alluvial charts were created using online tool RawGraphs 2.0 (https://www.rawgraphs.io/).

Relative contribution of A, B, and D subgenomes within expressed triads

To study triads expression, a total of 19,801 1:1:1 syntenic and non-syntenic homoeologous triads (representing a total of 59,403 genes) were analysed to quantify subgenome contributions (Ramírez-González et al., 2018). A triad was considered expressed when the sum of FPKM across its three homoeologs exceeded 0.5 ($FPKM_A + FPKM_B + FPKM_D > 0.5$), which also retains triads in which only one homoeolog was expressed and permits downstream classification of dominance (Ramírez-González et al., 2018). Using this criterion, 50,254 genes were expressed (Dataset_S1). Within each treatment, expression values were used as FPKM and triad-level normalisation was performed prior to relative-contribution calculations. For each expressed triad, the relative contribution of each homoeolog was computed as:

$$\text{expression}_A = FPKM_A/(FPKM_A + FPKM_B + FPKM_D),$$

$$\text{expression}_B = FPKM_B/(FPKM_A + FPKM_B + FPKM_D),$$

$$\text{expression}_D = FPKM_D/(FPKM_A + FPKM_B + FPKM_D)$$

where $FPKM_A$, $FPKM_B$ and $FPKM_D$ are the FPKM values for the A, B and D homoeologs after within-treatment normalisation. These relative contributions sum to 1 for each triad and were used for classification and plotting. Triads were classified into balanced, dominant or suppressed categories using thresholds adapted from (Ramírez-González et al., 2018). Ternary plots of normalised expression were generated using the ggtern R package (Hamilton and Ferry, 2018)

Expression patterns of DEGs common to single and combined stresses

Differentially expressed genes identified in single (e.g., eT, D) and combined (e.g., eT+D) stress treatments were categorised into six response modes – additive, synergistic, neutral, dominant, antagonistic, and equalisation – based on their $\log_2$FC values and associated variability (± standard deviation) (Shaar-Moshe et al., 2017). Briefly, in the additive mode, the $\log_2$FC under combined stress approximates the sum of the $\log_2$FCs from corresponding single stress treatments; in the synergistic mode, $\log_2$FC exceeds this sum. The neutral mode exhibits similar $\log_2$FC across all stress conditions. Conversely, antagonistic responses display opposite $\log_2$FC in combined versus single stresses, and equalisation occurs when the combined-stress $\log_2$FC resembles the sum of single-stress $\log_2$FCs but with opposing effects. Finally, in the dominant mode, the $\log_2$FC under single and combined stresses remains similar. Transcripts that did not fit these categories were classified as not assigned (NA).

Identification of potential treatment-specific marker genes

Treatment-specific genes were identified based on FPKM values. Genes were selected if they exhibited at least a 5-fold increase relative to control and a 2-fold increase compared with all other treatments. If an excessive number of genes met these criteria, the threshold for the difference from other treatments was raised to 5-fold.

Weighted gene co-expression network analysis (WGCNA)

Log_2FC values of DEGs from all treatments were used for WGCNA in R (Langfelder and Horvath, 2008). A soft-thresholding power (β) was set to 18 to meet the criteria for scale-free topology. Modules were defined with a minimum size of 30 genes, a cut height of 0.15, and an adjacency matrix dissimilarity threshold of 0.2. Module eigengenes were correlated with morpho-physiological traits at a significance level of $p \leq 0.05$. Modules with $|r| \geq 0.8$ or ≤ -0.8 and an adjusted p-value < 0.01 were subjected to further functional enrichment and trait association analyses. For gene prioritisation, within each selected module we computed within-module connectivity (degree; number of connections to other genes based on the adjacency/TOM) and designated the top 10 genes per module as "top" genes.

Transcription factors enrichment analysis

Transcription factor (TF) enrichment analysis was performed using the protein sequences of DEGs ($\log_2$FC > 1 or < -1, adjusted p-value < 0.01). These sequences were retrieved from EnsemblPlants BioMart (https://plants.ensembl.org/biomart/martview/), while TF families were identified using the PlantTFDB Prediction tool (https://planttfdb.gao-lab.org/prediction.php).

Statistical analysis of non-RNA sequencing data

Non-RNA-seq data were analysed for normality, followed by one-way or multi-way ANOVA with Tukey's HSD post hoc test ($p < 0.05$) using STATISTICA 13 (StatSoft).

Results

Morpho-physiological responses of wheat to single and combined factors

We measured a range of morphological and physiological parameters to evaluate the impact of different treatments (D, eT, eC and their combinations; Fig. 1A) on the phenotypic outcomes of wheat. These traits were subsequently grouped using hierarchical clustering (Fig. 2). The morphological traits analysed included plant height (PH), flag leaf length (FLL), shoot biomass (SBM), number of spikes (NoSP), spike biomass (SPBM), spike length (SPL), and husk weight (HUWt), as well as grain morphology (Fig. 2A–E, Figs. S1, S2). All drought-containing treatments – whether applied alone or in combination – clustered together (Fig. 2F). Among all combinations, the eT+D treatment caused the most pronounced negative effects, reducing PH by 18 %, FLL by 40 %, and SBM by 20 % relative to the control (Figs. S1). Drought alone demonstrated similar but less severe trends. In contrast, eC and eC+eT improved plant performance, increasing SBM by 8 % and 16 %, respectively, and enhancing NoSP and SPBM by 18–42 %. Notably, eC+eT caused a 6-fold increase in HUWt (Ctr = 0.6 g, eC+eT = 3.4 g).

Grain-related parameters included the number of grains per plant (NoG), grain weight (GW), thousand-grain weight (TGW), grain area (AR), grain length (GL), grain width (GW), grain circularity (CIR), grain periphery (PER), and the grain width-to-length ratio (GW/GL) (Fig. 2D, F and Figs. S2, S4). Under drought conditions, TGW and NoG decreased by 12 % and 15 %, respectively. Notably, eT+D reduced TGW by 27 % compared with the control but did not affect NoG. In contrast, eT and eC+eT increased NoG by 34 % and 28 %, respectively, while slightly

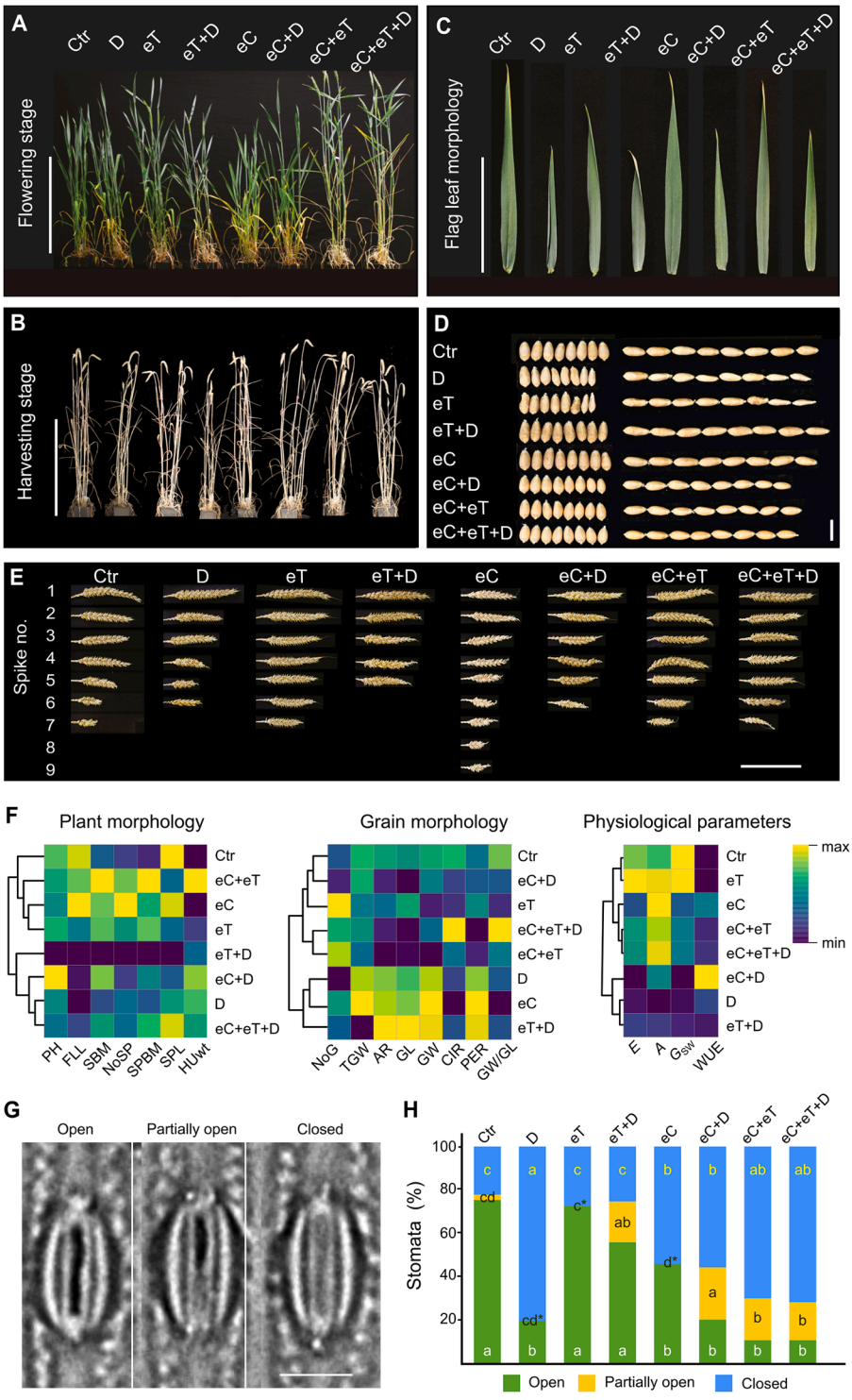

Fig. 2. Effects of individual and combined treatments on wheat performance.
(A, B) Representative images of wheat phenotypes at the flowering (A) and harvesting (B) stages under different treatment regimes. Scale bars, 30 cm. (C) Comparison of flag leaf morphology across treatments. Scale bar, 10 cm. (D) Representative images depicting grain width and length for each treatment. Scale bar, 10 mm. (E) Representative pictures of spikes collected from individual plants under each treatment. Scale bar, 10 cm. (F) Hierarchical clustering of plant morphology, grain traits, and physiological parameters. Morphological parameters: plant height (PH), flag leaf length (FLL), shoot biomass (SBM), number of spikes per plant (NoSP), spike biomass (SPBM), spike length (SPL), and husk weight (HUWt). Grain traits: number of grains per spike (NoG), thousand-grain weight (TGW), grain area (AR), grain length (GL), grain width (GW), circularity (CIR), periphery (PER), and grain width-to-length ratio (GW/GL). Physiological parameters: transpiration rate (*E*), photosynthesis rate (*A*), stomatal conductance (G_{SW}), and water-use efficiency (WUE). Source data are provided in Figs S1-S3. (G) Representative stomatal phenotypes categorised as open, partially open, or closed. Scale bar, 10 μm. (H) The percentages of open, partially open, and closed stomata represent mean values from three plants, with ≥500 cells evaluated per plant. ANOVA was performed separately for each stomatal phenotype. Different letters indicate statistically significant differences ($P \leq 0.05$, Tukey's post hoc test). The asterisks denote partially open stomata that occurred at a very low proportion (< 0.01 %) and are not visually represented.

decreasing TGW. Elevated CO_2 had the strongest positive effect, increasing NoG and TGW by 15 % and 11 %, respectively. Grain shape parameters were most affected by drought, eC, and eT+D.

Transpiration rate (*E*), photosynthetic rate (*A*), stomatal conductance (G_{SW}), and water-use efficiency (WUE) exhibited a distinct clustering pattern for drought-related treatments (D, eT+D, eC+D) (Fig. 2F and Figs. S3, S4). All drought-containing combinations significantly reduced *E* (by 63 % to 71 %) and G_{SW} (by 70 % to 80 %) compared to the control. In contrast, elevated temperature alone increased *E*, *A*, and G_{SW} by approximately 10 % to 30 %. Water-use efficiency (WUE) increased markedly under elevated CO_2 by 174 %. Moreover, the combined elevated CO_2 and drought treatment (eC+D) led to an even more pronounced enhancement in WUE, with an increase exceeding 320 % (Fig. S3), suggesting a synergistic effect of these factors on water-use optimisation.

We also analysed stomatal aperture status, categorizing stomata as open, partially open, or closed (Fig. 2G, H). Under control and single-factor treatments, stomata tended to be either fully open or completely closed. In control and eT conditions, 75 % of stomata were open and 25 % closed, whereas drought reversed this pattern (25 % open, 75 % closed). Under eC conditions, 45 % of stomata were open and 55 % closed. Importantly, all combined treatments resulted in a comparable proportion of partially open stomata, accounting for approximately 20 % across treatments. In the eT+D treatment, open stomata were more prevalent (57 %), whereas closed stomata were more common in other combinations, reaching 55 % in eC+D, 70 % in eC+eT, and 72 % in eC+eT+D.

Taken together, the most severe negative impacts on plant growth,

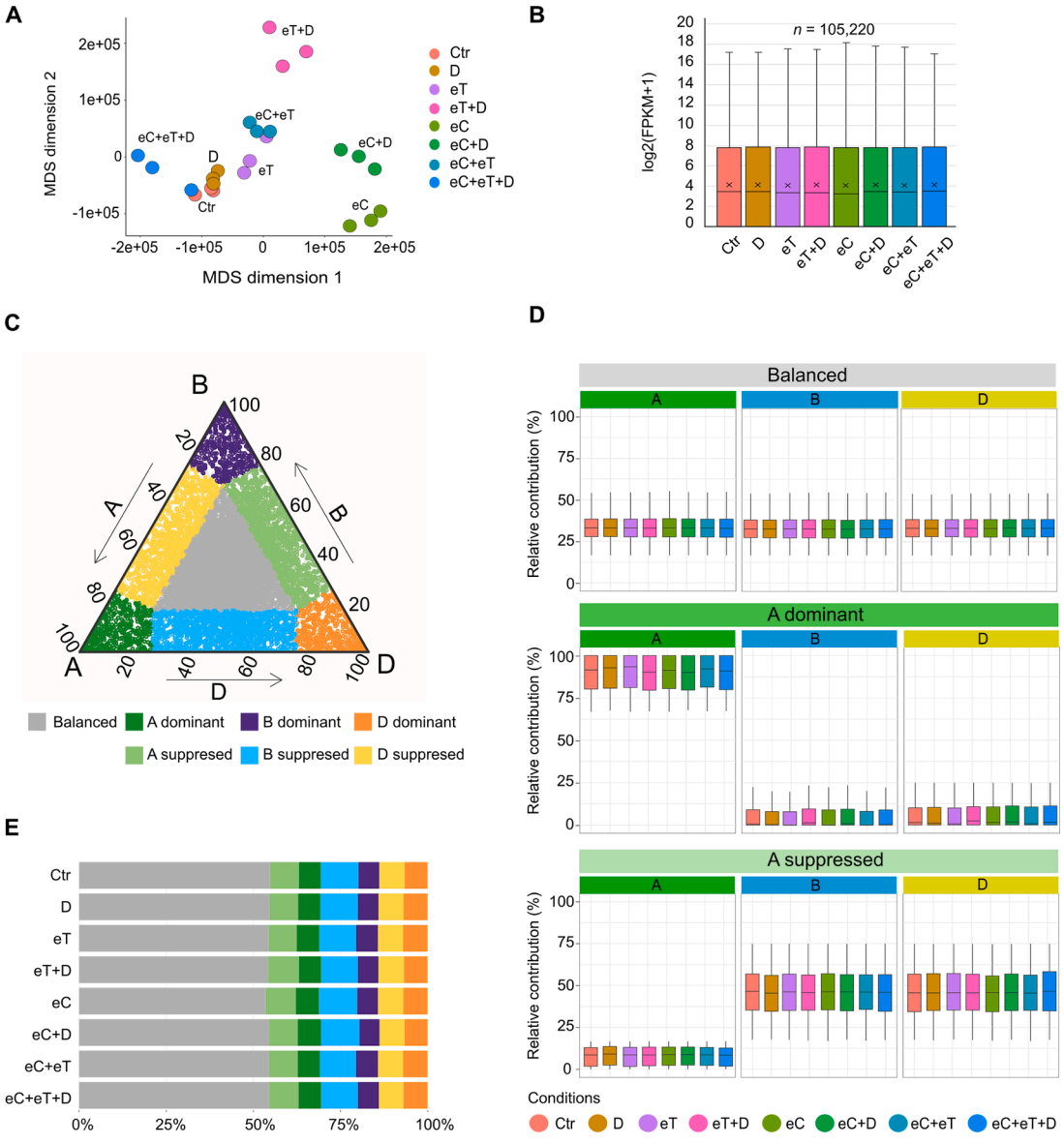

Fig. 3. Relative expression patterns of homoeologous triads across subgenomes.
(A) Multidimensional scaling (MDS) of 24 transcriptomes, with each point representing a color-coded biological replicate by treatment. Clustering reflects high similarity among replicates within each treatment. (B) Boxplots of gene expression levels (FPKM) for genes with non-zero expression. The box shows the interquartile range (IQR), with the median (line) and mean (cross). Whiskers extend to 1.5 times the IQR. (C) Ternary plot (control shown; cultivar Alana) of relative contributions (%) from A, B and D homoeologs in 1:1:1 triad. Each point is a triad; the centre (grey) indicates balanced A:B:D contribution; coloured sectors indicate dominance or suppression toward particular subgenomes. Axes show percentage contribution. (D) Boxplots showing the relative homoeolog contribution (%) for triads classified as balanced, A dominant or A suppressed across control and stress conditions (A subgenome shown; B and D subgenomes in Supplementary Fig. S7). (E) Proportion of triads classified as balanced, dominant or suppressed across control and treatments. Colours indicate categories as in (C).

biomass, and grain yield occurred under the eT+D and drought-only treatments. Conversely, elevated CO_2 consistently enhanced spike and grain traits, even under combined conditions.

Subgenome triad expression patterns in single and combined treatments

We next examined transcriptomic reprogramming under single and combined treatments using RNA-seq analysis of leaves collected at the flowering stage. Multidimensional scaling (MDS) revealed clear clustering of biological replicates according to treatment (Fig. 3A). Samples from the eC, eT+D, and eC+D treatments were markedly separated from the control, indicating substantial transcriptional shifts, while the drought-treated and eC+eT+D samples clustered more closely with control samples. Gene expression levels (FPKM) were generally consistent across treatments, with median expression ranging from 3.24 (eT+D) to 3.36 (control) (Fig. 3B, Dataset-S2. Notably, approximately 40 % of expressed genes in each treatment exhibited very low (0–1 FPKM) expression levels (Fig. S5).

Wheat is an allohexaploid with three subgenomes AABBDD; to quantify subgenome contributions we performed a ternary analysis of 1:1:1 homoeologous triads and classified triads as balanced (near-equal A:B:D contribution), dominant (one homoeolog predominates) or suppressed (one homoeolog is reduced) (Fig. 3C–D, Figs. S6–S9). Across control and stress conditions ~54–57 % of triads were balanced, indicating broadly conserved expression from the A, B and D subgenomes. A minority of triads showed biased expression: A dominant ≈ 7–8 % (A suppressed ≈ 4–5 %), B dominant ≈ 10–12 % (B suppressed ≈ 4–5 %), and D dominant/suppressed each ≈ 5 % (Fig. 3E, Fig. S7). These proportions were broadly similar across treatments, with only modest, treatment-dependent reallocations of homoeolog contribution (Fig. 3E).

In summary, treatment-specific transcriptomes coexist with largely balanced 1:1:1 triads; minor, treatment-dependent homoeolog biases

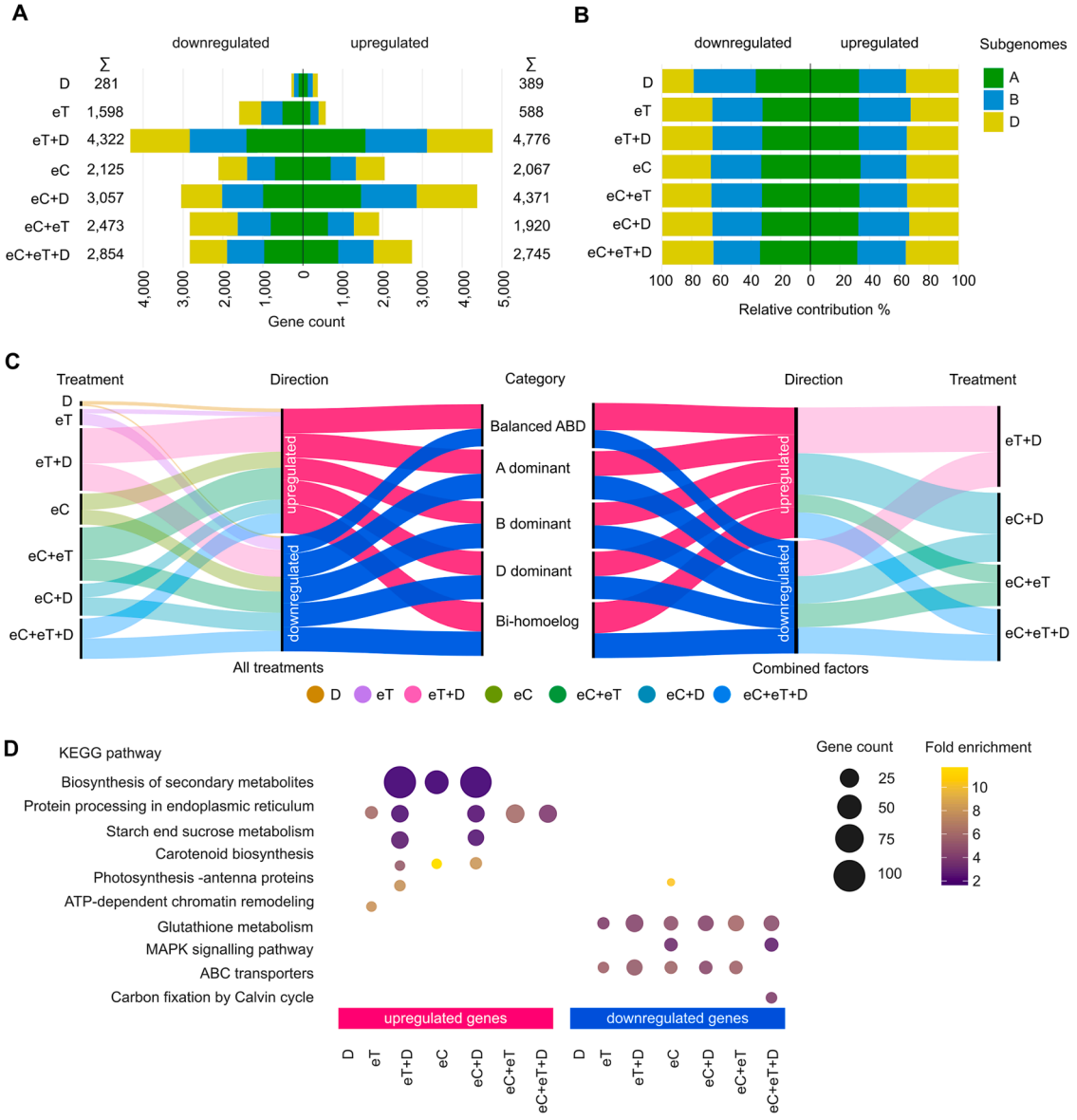

Fig. 4. Global transcriptomic profiles and pathway responses.
(A) Bar plots showing the total number (Σ) of differentially expressed genes (DEGs) assigned to the A, B and D subgenomes for each treatment. DEGs were called after homoeolog-bias correction (see Methods). Data for subgenomes are provided in Supplementary Table S3. (B) Stacked-bar representation of the relative contribution (%) of A, B and D DEGs for each treatment based on the counts in (A). (C) Alluvial diagrams linking treatment, direction of regulation (down-/upregulated) and subgenome (A/B/D). Stream width is proportional to the number of DEGs flowing between categories. (D) Bubble plot of selected KEGG pathways enriched among up- and down-regulated genes. Only DEGs retained after homoeolog-bias correction ($\log_2$FC > 1 or < −1, adjusted p -value < 0.01) were included.

occur, but no genome-wide subgenome shift was detected.

Transcriptomic and pathway responses of wheat to single and combined treatments

We analysed differentially expressed genes (DEGs) after correcting for homoeolog bias (Fig.4A, Table S3). Among the single-factor treatments, eC elicited the largest response (2067 up- and 2125 down-regulated genes), followed by eT, which triggered 588 up- and 1598 down-regulated genes. In contrast, drought (D) induced a smaller transcriptional response (389 up-, 281 downregulated genes Two-factor combinations provoked substantially larger transcriptomic shifts: eT+D (4776 up- and 4322 down-regulated genes) and eC+D (4371 up- and 3057 down-regulated genes) showed the highest DEG counts, whereas eC+eT elicited 1920 up- and 2473 down-regulated genes. The three-factor treatment (eC+eT+D) produced an intermediate response (2745 up- and 2854 down-regulated genes). Across treatments, upregulated DEGs were distributed approximately equally among the A, B and D subgenomes (≈ one-third each). A small deviation from this pattern was observed for downregulated genes under drought, which were skewed toward the A and B subgenomes (A: 37 %, B: 42 %, D: 21 %) (Fig. 4B).

To integrate gene- and triad-level behaviour, we constructed alluvial diagrams (Fig. 4C). Up-regulated DEGs were broadly distributed across triad classes (≈ 20 % in balanced ABD, A, B- and D-dominant, and bi-homoeolog categories), whereas down-regulated DEGs showed a larger share of biased triads (balanced ≈ 10 %; other categories ≈ 20–22 %). The largest flows into both balanced and biased categories derived from combined-stress treatments (notably eT+D and eC+D).

KEGG pathway enrichment (homoeolog-corrected) revealed treatment-specific signatures (Fig. 4D, Table S4). Elevated temperature was associated primarily with protein processing in the endoplasmic reticulum and chromatin-remodelling terms. Elevated CO_2 enriched pathways related to secondary-metabolite and carotenoid biosynthesis. Double stresses (eT+D, eC+D) showed broad enrichment across several pathways — including secondary-metabolite biosynthesis, ER protein processing, sugar metabolism and carotenoid biosynthesis — and eT+D was uniquely enriched for photosynthetic antenna proteins. By contrast, eC+eT and the triple treatment were dominated by ER protein-processing enrichment. Across many conditions, glutathione metabolism was recurrently downregulated and ABC transporter genes were frequently repressed.

Overall, multi-factor treatments induced stronger and broader transcriptional responses than single factors. Among single factors, elevated CO_2 had the most pronounced effect, whereas the eT+D and eC+D combinations triggered the largest transcriptomic reprogramming among two-factor treatments.

Unique, shared, and potential marker genes in single and combined treatments

To differentiate between unique and shared transcriptional responses, we generated UpSet plots (Fig. 5A). Drought alone resulted in only 131 unique DEGs, while eT and eC induced 387 and 707 unique DEGs, representing 0.4 %, 1.1 %, and 2.1 % of the total DEGs, respectively (Fig. 5B). In contrast, combined treatments produced substantially more unique genes – for example, eT+D yielded 3321 unique DEGs (10 %) and eC+D 2066 (6.1 %) (Dataset_S3). GO enrichment analysis of biological processes for triad-collapsed DEGs revealed distinct, treatment-specific patterns (Fig. 5C and Figs. S10, S11). Among the up-regulated categories, response to heat was strongly enriched under elevated temperature and in all combinations that included heat. Chromatin remodelling was also enriched under eT, indicating activation of chromatin-based regulatory programs during thermal stress. Chloroplast-related processes – chloroplast organization and photosynthesis – were enriched under elevated CO_2 and eC-containing combinations, consistent with stimulation of chloroplast/photochemical functions. In contrast, down-regulated genes consistently showed enrichment for cell communication, pointing to a general attenuation of intercellular signalling across stresses. Transmembrane transport appeared in both the up- and down-regulated categories depending on treatment, indicating a reconfiguration of transport capacity (induction of specific transporters accompanied by repression of others).

Several dozen genes exhibited distinct expression patterns under specific treatments and may serve as potential treatment-specific marker genes (Fig. 5D, genes mentioned in the text). Across the entire experiment, we detected marker candidates in every treatment, ranging from two upregulated genes in eT to 291 downregulated genes in eT+D. For clarity, only the most significant representative gene for each treatment is shown. The complete list of candidates is provided in Dataset_S4. For instance, drought alone caused an 11-fold increase in the expression of *MITOGEN-ACTIVATED PROTEIN KINASE KINASE KINASE 17* (*MAP3K17; TraesCS1B03G1045900*) compared to the control, consistent with the observed enrichment of the MAPK signalling cascade. Elevated CO_2 triggered an 8-fold increase in *AQUAPORIN PIP2–6* (*PIP2–6; TraesCS5D03G0192000)* expression, potentially enhancing CO_2 diffusion across cell membranes and photosynthetic efficiency (Xu et al., 2019). Elevated temperature led to a five-fold upregulation of *PROTEIN ARGONAUTE 4A* (*AGO4A; TraesCS7A03G1266600*), which may play a role in regulating heat-activated transposable elements (Miloro et al., 2024). The eT+D treatment induced a more than 2500-fold increase in *PM19L* (*TraesCS1B03G1045900*), a plasma membrane protein gene linked to transmembrane transport (Fig. 5D). Additionally, the *CHLOROPHYLL A–B BINDING PROTEIN OF LHCII* gene (*TraesCS1D03G0506300*) was upregulated 17-fold relative to control plants (Dataset_S4), suggesting enhanced chlorophyll accumulation and light-harvesting capacity (Pietrzykowska et al., 2014).

The combination of eC+eT caused a nearly 500-fold increase in *HEAT SHOCK PROTEIN 1* expression (*16.9 kDa HSP1; TraesCS3D03G0079600*), aligning with heat-response GO biological process (Fig. 5C), and likely contributing to thermotolerance by stabilising protein structure and preventing heat-induced aggregation. Under eC+D, *PEROXIDASE 5-LIKE* (*PRX5; TraesCS4B03G0539200*) expression was upregulated 32-fold, indicating a key role in mitigating oxidative stress by scavenging reactive oxygen species (ROS) and maintaining cellular redox balance (Su et al., 2020). The three-factor treatment (eC+eT+D) induced a 9-fold increase in *GLUTATHIONE S-TRANSFERASE 1* expression (*GSTF1; TraesCS2A03G0085500*), likely enhancing the plant's antioxidant capacity through glutathione conjugation and supporting abiotic stress resilience (Chen et al., 2012).

To test whether the subgenome carrying a putative marker also dominates expression at its locus, we visualised A/B/D partitioning with ternary plots (Fig. 5E and Fig. S12). For several loci, the designated marker homoeolog was the major contributor – for example *PM19L* (chromosome 5B), *HSP1* (chromosome 3D) and *GSTF1* (chromosome 2A) (Fig. 5E) – whose marker copies also showed the largest fractional contribution within their gene triads. In other cases, a non-marker homoeolog contributed more to total FPKM at that locus (e.g. *PIP2–6* with $A > D$ under eC; *PRX5* with $D > B$ under eC+D) (Fig. S12), yet these copies did not satisfy our stringent definition of "treatment-specific marker" ($\geq$ 5-fold vs control and $\geq$ 2-fold vs all other treatments, or $\geq$ 5-fold if an excess of candidates) across regimes and were therefore not classified as markers. This distinction clarifies why the highest-expressed homoeolog in the ternary plot is not always the one flagged as a marker; marker status is based on cross-treatment selectivity, whereas the ternary plot summarizes within-gene dosage among homoeologs in the focal treatment. This observation was supported by public RNA-seq data showing *PRX5* homoeologs expression descending in the pattern 4D > 5A > 4B (Borrill et al., 2016).

The candidate marker genes identified under specific treatments underscore core pathways involved in environmental adaptation and represent promising targets for breeding wheat with enhanced resilience

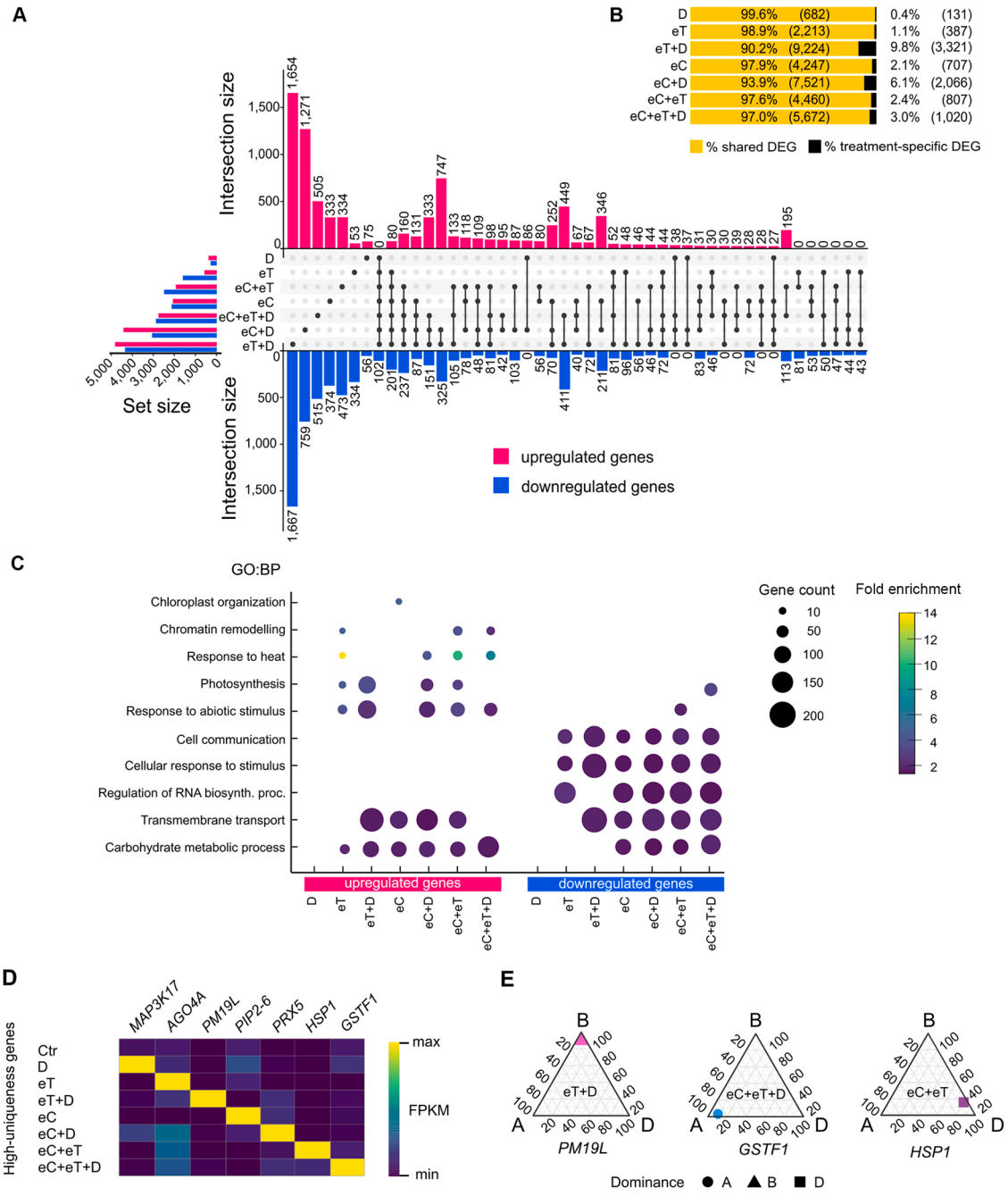

Fig. 5. Unique and shared transcriptomic responses.
(A) UpSet plots displaying upregulated (top) and downregulated (bottom) differentially expressed genes (DEGs) across treatments. The x-axis shows the total number of DEGs, while the y-axis indicates DEGs unique to single treatments (single dots) or shared across combined treatments (connected dots). (B) Bar chart showing the percentage of unique and shared significant DEGs ($\log_2$FC > 1 or < 1, adjusted p-value < 0.01) for each condition, with the number of DEGs indicated in brackets. (C) Matrix bubble plot showing the most enriched biological processes (BP) from Gene Ontology enrichment analysis (adjusted $p < 0.01$) across the unique (condition-specific) genes identified in (B). (D) Examples of highly expressed genes specific to certain conditions. *High-uniqueness* genes were defined as those showing ≥ 5-fold higher expression relative to the control and ≥ 2-fold higher expression compared to all other treatments. If an excessive number of genes met these criteria, the threshold for the difference from other treatments was raised to 5-fold. Gene symbols and IDs (listed from top to bottom): *MITOGEN-ACTIVATED PROTEIN KINASE KINASE KINASE 17 (MAP3K17, TraesCS1B03G1045900)*, *PROTEIN ARGONAUTE 4A* (*AGO4A, TraesCS7A03G1266600*), *PLASMA MEMBRANE PROTEIN 19 (PM19L, TraesCS5B03G1369900*), *AQUAPORIN PIP2–6* (*PIP2–6, TraesCS5D03G0192000*), *PEROXIDASE 5-LIKE (PRX5, TraesCS4B03G0539200*), *16.9 kDa CLASS I HEAT SHOCK PROTEIN 1* (*16.9 kDa HSP1, TraesCS3D03G0079600*), *GLUTATHIONE S-TRANSFERASE 1* (*GSTF1, TraesCS2A03G0085500*). (E) Ternary plots presenting relative contributions of A, B and D subgenomes to expression of selected genes from (D). Each point is a gene-treatment mean expressed as a fraction of the sum of FPKM for its three homoeologs ($A + B + D = 1$). Missing homoeolog or undetected expression was treated as 0. Gridlines mark 20 % increments. Proximity to a vertex indicates dominance of that subgenome. Remaining genes from (D) are shown in Supplementary Fig. S12.

to future climate conditions.

Response-mode partitioning of shared DEGs under combined stress

Using the workflow described in (Shaar-Moshe et al., 2017), all shared DEGs (Fig. S13) were categorised into one of five response modes – additive, synergistic, neutral, dominant, or not assigned (NA). Antagonistic and equalisation patterns were not detected (Fig. 6A–B, Dataset_S5). In two-factor treatments, dominance or neutrality generally prevailed, although the distribution varied depending on the specific combination. For example, in eC+eT, approximately one-third of DEGs followed a dominant pattern (≈ 32 %), while another ≈ 29 % responded additively; synergistic responses were rare (<1 %). In eC+D, additive responses were more prominent (approximately 37 %), whereas dominance and neutrality each accounted for ≈ 25 % (Fig. 6B). The eT+D treatment resulted in a more balanced profile: dominant (≈ 29 %), neutral (≈ 27 %), and additive (≈ 23 %), with approximately 2 % of DEGs showing synergistic behaviour. Adding a third factor substantially altered this distribution. Under eC+eT+D treatment, dominance remained the most frequent response (≈ 47 %), while additive responses dropped to ≈ 4 % and no synergistic behaviour was detected.

In summary, paired stresses elicit dominant, additive and neutral responses in wheat, while addition of the third factor strengthens dominance and diminishes additivity, with synergistic mode remaining rare.

Co-expression network analysis reveals key gene modules regulating morpho-physiological traits under combined environmental conditions

We performed weighted gene co-expression network analysis (WGCNA) on RNA-seq data from both single and combined treatments to identify co-regulated clusters. This analysis revealed 56 distinct modules, each representing genes with highly correlated expression profiles across treatments (Fig. 7A, Fig. S14).

To associate gene modules with morpho-physiological traits (Fig. 2), we correlated module eigengenes with measured trait values. Several modules showed strong correlations (Pearson's $|r| \geq 0.8$, adjusted $p < 0.01$), suggesting potential regulatory links (Fig. 7B). For instance, plant height (PH) was strongly associated with modules M53, M54, and M55 (Fig. 7B,C). Similarly, shoot biomass (SBM) was positively correlated with modules M2, M43, and M54, which were upregulated under eC+eT but downregulated under eT+D, suggesting treatment-specific regulatory mechanisms influencing growth. For thousand grain weight (TGW), module M46 demonstrated the strongest correlation. Photosynthetic rate (*A*) also correlated with modules M2, M43, and M54, which were upregulated under eC and eC+eT but suppressed under eT+D – paralleling the observed reductions in PH, TGW, and *A* (Fig. 2F, Fig. 7C and Figs. S1–S3).

To gain mechanistic insight, we inspected high-connectivity genes within trait-associated modules (Fig. 7D, Fig S15). Modules M2 and M43 were both positively associated with SBM and photosynthetic rate (*A*) (Dataset_S6). Module M2 includes genes upregulated by eC, eC+D and eC+eT and is anchored by candidate hubs such as an *ABC TRANSPORTER G FAMILY (ABCG, TraesCS5D03G0351500)*, an *FAO1-like ALCOHOL OXIDASE* (*FAO1, TraesCS1D03G0261600*) and a *PHOSPHATIDYLINOSITOL-TRANSFER PROTEIN* (*PITP, TraesCS5D03G1174400*) (Fig. 7D). Module M43 is upregulated under eC, eC+eT and eC+eT+D (and, for some genes, also by eT) and is enriched for stress-responsive genes encoding HSP18.9 (*TraesCS6B03G0192300*) a LATE EMBRYOGENEIS ABUNDANT-2 protein (*LEA-2, TraesCS2A03G1353100*), a JASMONATE-INDUCED OXYGENASE-like enzyme (*JOX-2, TraesCS3A03G0599100*) and the bHLH156 (*TraesCS2D03G0517800*) transcription factor (Fig. 7D). These contrasting hub profiles suggest distinct mechanisms: M2 hubs are consistent with enhanced transport and metabolic activity under elevated CO_2, whereas M43 hubs implicate protein protection, hormone-linked signalling and transcriptional control in the CO_2-responsive stress response.

Overall, these module–trait associations and their hub genes provide candidate targets for functional validation and for breeding or biotechnological strategies aimed at improving growth and photosynthetic resilience under complex environmental stresses.

Combined treatments amplify transcription factor responses

Transcription factors (TFs) are proteins that regulate gene expression during plant growth and defence responses. We identified significantly altered TFs ($log_2FC > 1$ or < -1, $p < 0.01$) across all treatments (Fig. 8 and Fig. S16). Combined treatments, particularly eC+D, eT+D, and eC+eT+D, resulted in substantial enrichment of upregulated TF families (Fig. 8A, Dataset_S7). Notable families included bHLH, bZIP, ERF, MYB, MYB-related, NAC, WRKY, and HSF, all known to participate in stress signalling and transcriptional control.

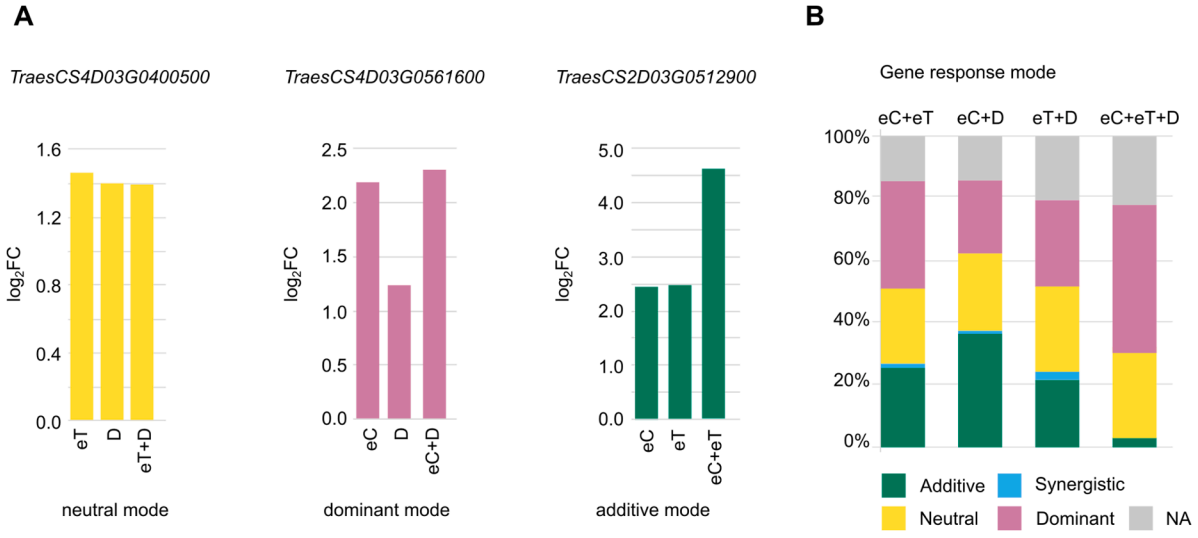

Fig. 6. Transcriptional response modes among shared and combination-specific DEGs.
(A) Response mode partitioning of shared DEGs among transcriptional patterns in two-factor and three-factor treatment combinations. Data underlying the plots are provided in Supplementary Dataset_S5. (B) Representative example genes illustrating response mode across double and triple stresses. Plots show normalized expression (log_2FC) per treatment.

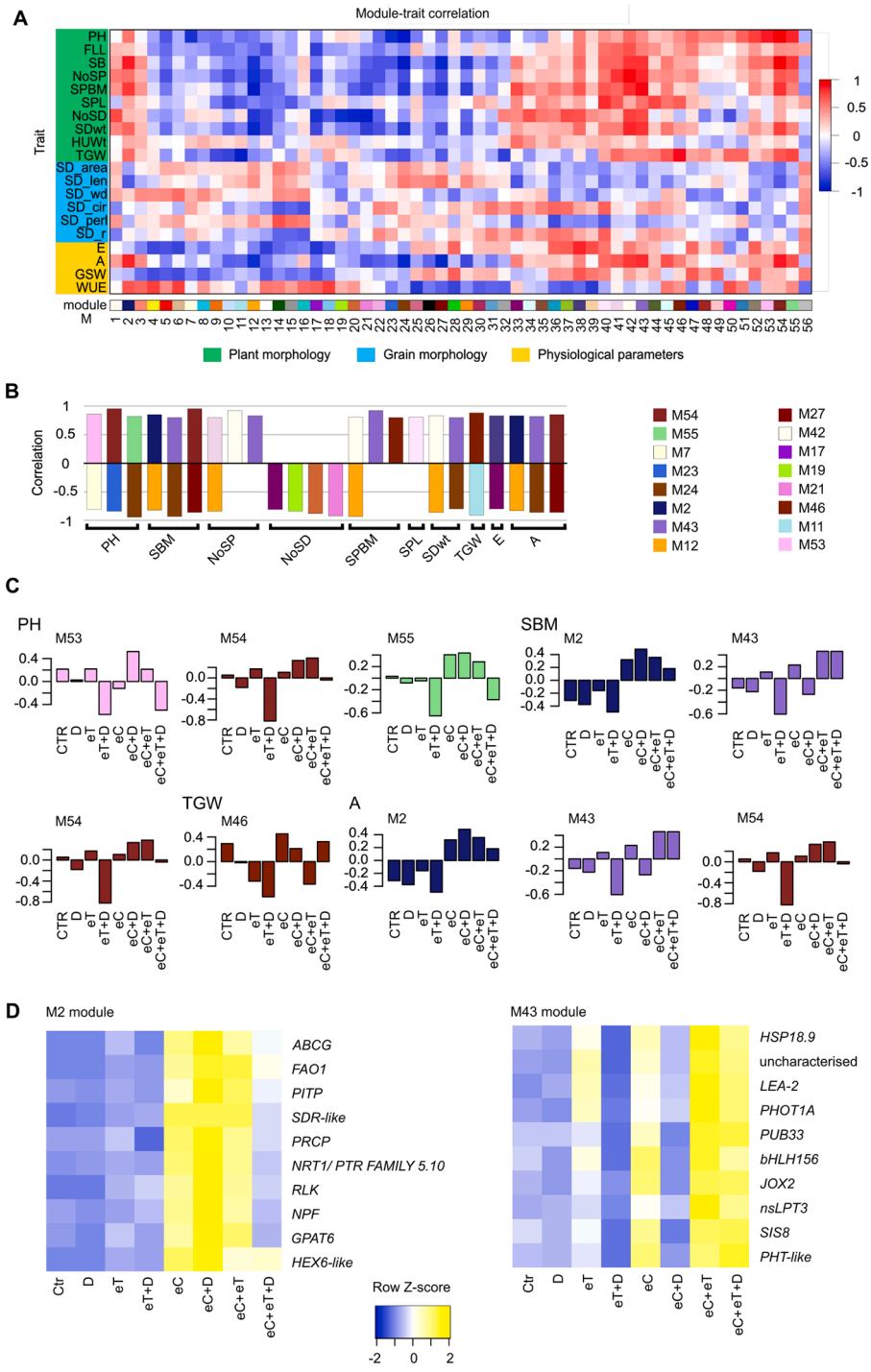

Fig. 7. Gene co-expression network analysis and its correlation with morpho-physiological traits.
(A) Module-trait correlation matrix. Heatmap displays both positive and negative correlation between modules identified using Weighted Gene Co-Expression Network Analysis (WGCNA) and phenotypic traits, measured during experiments. M stands for module number. Plant morphology parameters (green): PH (plant height), FLL (flag leaf length), SBM (shoot biomass), NoSP (number of spikes), SPBM (spike biomass), SPL (spike length), and HUWt (husk weight).Grain parameters (blue): NoG (number of grains per spike), TGW (thousand-grain weight), AR (grain area), GL (grain length), GW (grain width), CIR (seed circularity), PER (grain periphery), and GW/GL (grain width-to-length ratio). Physiological parameters (yellow): *E* (transpiration rate), *A* (photosynthesis rate), G_{SW} (stomatal conductance), and WUE (water-use efficiency).(B) Modules with a gene significance (Pearson correlation coefficient) $\geq 0.8/ \leq 0.8$ with morpho-physiological traits. Feature descriptions as in (A). (C) Selected gene modules with positive trait correlation (Pearson correlation coefficient ≥ 0.8) showing eigengene expression under individual treatments. (D) Representative top-ranked genes from selected WGCNA modules shown as heatmaps. For each module, rows are ordered top-to-bottom by intramodular connectivity. Remaining module genes are shown in Supplementary Fig. S15. Intramodular connectivity was calculated using WGCNA and top genes were selected by highest intramodular degree.

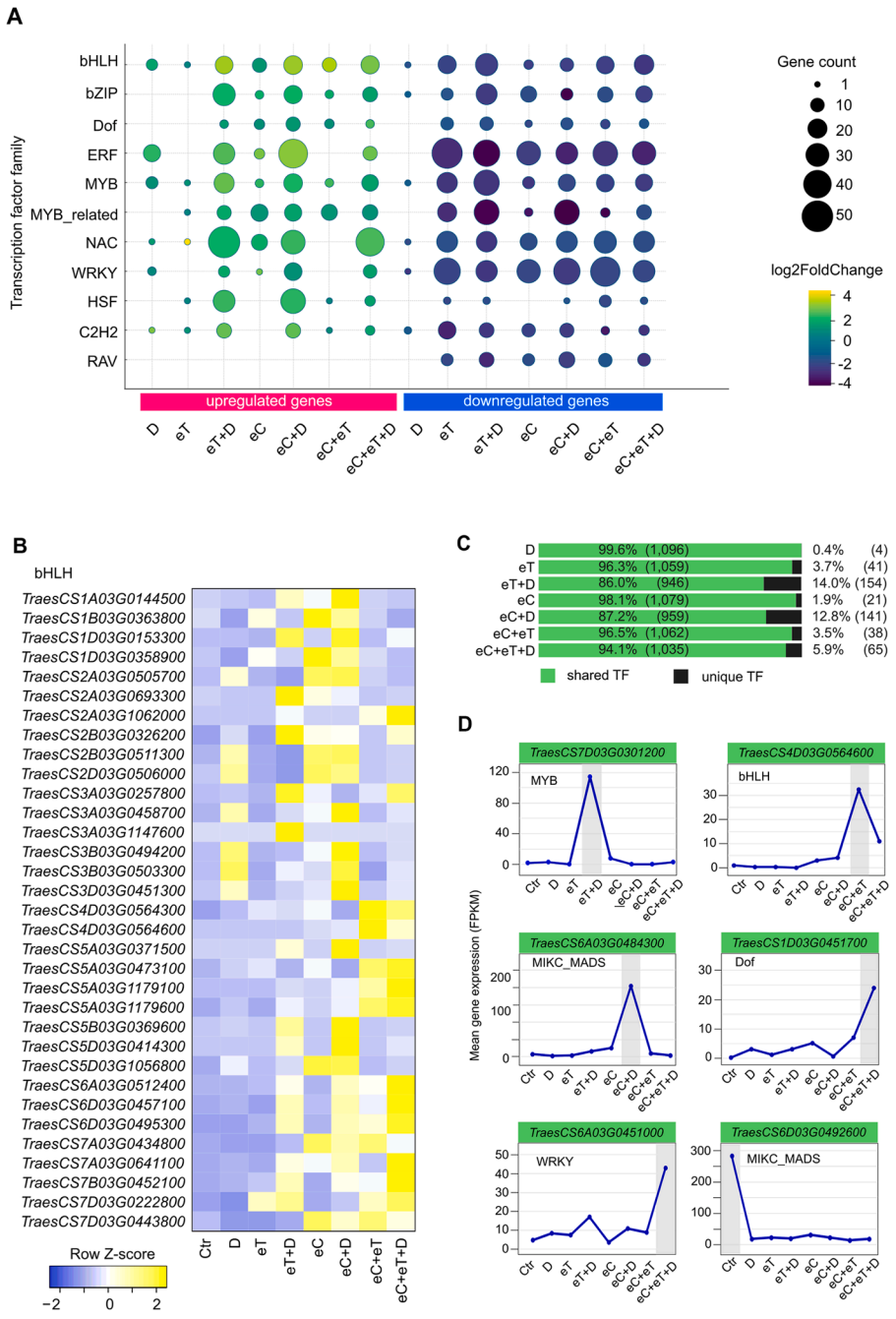

Fig. 8. Transcription factor enrichment.
(A) Matrix bubble plot illustrating the most enriched transcription factor (TF) families. (B) Heatmap displaying expression levels of bHLH family members that were overrepresented under specific treatment conditions. (C) Bar chart showing the proportion of shared and condition-specific significant TFs for each treatment, with the number of TFs indicated in brackets. (D) Examples of potentially novel regime-specific TFs. Conditions with unique expression are shaded in grey.

Most treatments exhibited downregulated TF families; however, drought alone induced minimal downregulation, underscoring differential regulatory responses between single and combined treatments. Comparative analysis revealed significant overlap of upregulated TFs across different treatments (Fig. 8B, C), reflecting similar patterns observed for protein-coding genes (Fig. 5B). However, a subset of TFs was uniquely responsive to specific combinations: 154 (14 %) in eT+D, 141 (13 %) in eC+D, and 65 (6 %) in eC+eT+D. For example, ERF, WRKY, MIKC_MADS, and HSF were specific to eC+D; ERF, bZIP, and NAC to eT+D; and NAC dominated the uniquely responsive TFs under eC+eT+D (Figs. S17, S18, Dataset_S7).

Several TFs also exhibited markedly higher expression under particular combinations of growth conditions (Fig. 8D). For instance, MYB (*TraesCS7D03G0301200*) was exclusively found in eT+D, MIKC_MADS (*TraesCS6A03G0484300*) in eC+D, while WRKY (*TraesCS6A03G0451000*) and Dof (*TraesCS1D03G0451700*) were most strongly induced under eC+eT+D. In contrast, several TFs were consistently downregulated across all treatments (Fig. 8D), for example MIKC_MADS (*TraesCS6D03G0492600*), the latter being an orthologue of *Arabidopsis thaliana AGAMOUS-LIKE 16*, a TF associated with developmental processes.

Altogether, these results underscore the crucial roles of major TF families – including bHLH, bZIP, ERF, WRKY, NAC, and HSF – in orchestrating multifactorial stress responses. The identification of

uniquely expressed TFs offers valuable insights into treatment-specific regulatory networks and points to potential targets for enhancing crop resilience.

Discussion

Our results split into two complementary themes: structural features of the wheat genome and the biological strategies wheat used to cope with single and combined stresses.

Genome structure and transcriptional strategies underlying single- and combined-stress responses

Bread wheat is an allohexaploid with three subgenomes (A, B and D). In cultivar Alana, most 1:1:1 homoeologous triads remained balanced (~ 54–57 %) across control and stress conditions (RNA collected from leaves sampled at flowering), whereas a higher balanced fraction (~ 70 %) has been reported for flag leaves in Chinese Spring cultivar (Ramírez-González et al., 2018). This difference likely reflects cultivar, tissue or developmental effects (true leaf vs flag leaf) rather than a fundamental inconsistency. A minority of triads showed A-, B- or D-biased expression; these biased triads represent a more plastic subset that can be selectively recruited by stress without provoking genome-wide reprogramming. Notably, stress can convert previously stable (tissue-specific) triads into dynamic, biased ones, indicating that homoeolog partitioning is itself responsive to environmental cues (Ramírez-González et al., 2018). Several condition-specific marker genes identified here are subgenome-specific, confirming that biologically important responses can be resolved at the homoeolog level. Mechanisms that could underlie such targeted recruitment include *cis*-regulatory variation, differential promoter responsiveness, trans-acting factors and epigenetic modulation (Concia et al., 2020).

A further key finding concerns how shared DEGs respond to single versus combined stresses. Using the additive/synergistic/neutral/dominant classification, two-factor combinations showed broadly similar frequencies of dominant, additive and neutral responses (each ≈ 20–30 %, treatment-dependent), whereas genuine synergy was rare (< 2 %). In contrast, the three-factor treatment (eC+eT+D) exhibited markedly higher dominance (47 %) and a sharp decline in additive responses (4 %), with no detectable synergy. Thus, roughly one in six shared DEGs under triple stress exhibited supra-additive expression that could not be predicted from single-stress responses. These results suggest that, with two concurrent factors, wheat generally either activates one prevailing transcriptional programme (dominance) or maintains largely independent regulation of each stress (neutrality). We interpret this shift as evidence that higher-order stress combinations engage additional layers of cross-talk – among ABA/JA/SA/ethylene signalling, and MAPK pathways – that are not fully activated under single or paired stresses. Under such conditions, a third factor can remove pathway antagonism or promote cooperative action of transcription factors and co-regulators, resulting in transcript levels that exceed additive expectations. This interpretation is consistent with reports that stress combinations generate unique, non-additive transcriptomes and that emergent (often synergistic) responses become more likely as the number of concurrent stresses increases (Zandalinas and Mittler, 2022; Atkinson and Urwin, 2012; Suzuki et al., 2014).

Combined elevated temperature and drought severely reduce wheat performance

Our results demonstrate that the simultaneous exposure to eT+D had the most detrimental effects on wheat growth and yield among all treatments. Key agronomic traits, such as plant height (PH), flag leaf length (FLL), shoot biomass (SBM), and thousand-grain weight (TGW), exhibited substantial declines compared to the control. Notably, the 40 % decline in FLL indicates a loss of photosynthetically active surface area, likely contributing to impaired grain filling and the observed 27 % decrease in TGW. These morphological changes are consistent with earlier reports indicating that the effects of combined heat and drought strongly reduce biomass accumulation and yield components in cereals (Khaliq et al., 2008; Mahmood et al., 1991).

At the physiological level, transpiration decreased by 65 %, consistent with a drought-induced water conservation strategy (Pflüger et al., 2024). Interestingly, while the proportion of fully open and fully closed stomata remained similar, a substantial increase in partially open stomata suggests a physiological compromise between opposing demands: facilitating evaporative cooling under high temperatures and minimizing water loss during drought (Merilo et al., 2014).

At the molecular level, eT+D triggered the highest number of DEGs among all treatments, indicating extensive transcriptomic reprogramming and activation of stress-response pathways. Gene ontology enrichment analysis of unique DEGs revealed the upregulation of genes related to photosynthesis, transmembrane transport, and abiotic stress response, suggesting metabolic adjustments to support cellular homeostasis. Among these, *PM19L*, coding for a plasma membrane protein involved in ABA (abscisic acid) signalling, was upregulated by more than 2500-fold. Such robust induction suggests a key role in enhancing drought and heat tolerance by modulating ABA-mediated responses (Meng et al., 2022; Rerksiri et al., 2013). In parallel, a 17-fold increase in *CHLOROPHYLL A-B BINDING PROTEIN OF LHCII* indicates an adaptive mechanism to maintain photosynthetic efficiency under stress. LHCII proteins form the core of the light-harvesting complex, capturing and transferring excitation energy to photosystems I and II. Under stress conditions such as heat and drought, their reversible phosphorylation enables dynamic redistribution of energy between photosystems, while structural roles in granal membrane adhesion and involvement in photoprotective processes – such as energy-dependent quenching – help prevent photodamage and maintain redox balance (Xu et al., 2012; Wang et al., 2023; Yang et al., 2000).

Transcription factor (TF) analysis revealed a strong upregulation of MYB family genes, which are known to regulate stomatal responses through ABA-dependent pathways (Jung et al., 2008; Cominelli et al., 2005). The co-induction between *OsPM19L* and MYB TFs suggests a coordinated regulatory mechanism linking ABA signalling with stomatal control and water-use efficiency (Yao et al., 2018). However, despite these physiological and molecular adjustments, yield losses under eT+D remained severe, underscoring the insufficient stress responses and highlighting the need for breeding strategies aimed at enhancing thermotolerance and drought resilience in wheat (Reynolds et al., 2021; Xiong et al., 2024).

Elevated CO_2 enhances wheat growth, yield, and physiological efficiency

In contrast to the detrimental effects of eT+D, elevated CO_2 (eC) alone had a positive effect on wheat growth and productivity (Vanaja et al., 2024; van der Kooi et al., 2016). Under CO_2-enriched conditions, plants produced significantly more SBM, spikes, and grains per plant, along with higher TGW, despite a modest 3 % reduction in PH. This slight reduction may reflect a shift in assimilate allocation from vertical stem elongation toward the development of photosynthetically active tissues and reproductive organs. In addition to these aboveground improvements, elevated CO_2 has also been widely associated with enhanced root system development (Bach and Gojon, 2023), which may contribute to improved water and nutrient acquisition under both optimal and stress conditions.

At the physiological level, eC substantially improved WUE by 174 %. This increase reflects a 22 % rise in net photosynthetic rate combined with reduced stomatal conductance by 64 %, which directly lowered transpirational water loss. Similar patterns have been observed in free-air CO_2 enrichment (FACE) studies (O'Leary et al., 2015; Ainsworth and Long, 2005; Cao et al., 2022), where elevated CO_2 enhanced both yield and WUE, an effect commonly referred to as CO_2 fertilisation.

Transcriptomic data further support these physiological observations. We detected significant upregulation of *AQUAPORIN PIP2–6*, a gene encoding a membrane channel protein involved in regulating water transport. Increased *AQUAPORIN PIP2–6* expression may enhance hydraulic conductivity, facilitate efficient water transport and contribute to ABA-triggered stomatal closure (Grondin et al., 2015), thereby improving WUE observed under elevated CO_2 conditions. The upregulation of aquaporins has been associated with adjusted stomatal movements and enhanced WUE in various species, even under eC conditions (Sade et al., 2010; Avila et al., 2020; Zhang et al., 2020; Maurel et al., 2016).

Together, these morphological, physiological, and molecular changes suggest that eC reprograms wheat metabolism to optimise carbon assimilation and WUE (Cao et al., 2022; Padhan et al., 2020). The integration of increased photosynthetic activity with improved resource allocation results in significant yield gains, which may partially compensate for the negative effects of future climate-induced stressors on global crop production (Long et al., 2006). However, the extent to which elevated CO_2 can mitigate the negative impacts of additional stressors such as heat and drought remains a critical question – addressed in the following section.

Elevated CO_2 partially mitigates damage from elevated temperature and drought

Given its beneficial effects, we next assessed whether elevated CO_2 could alleviate the negative impacts of combined drought and heat. Under drought conditions, eC significantly improved WUE by 116 %, driven by a 28 % reduction in transpiration and a 52 % increase in photosynthetic rate. This suggests that elevated CO_2 can partially counteract the limited water availability caused by drought (Zinta et al., 2014; Wang et al., 2022). The mitigation effects were even more pronounced under the three-factor treatment (eC+eT+D), where key morphological and physiological traits – including plant height, thousand grain weight, and photosynthetic rate – showed significant improvement compared to the eT+D combination. This improvement may be attributed to the ability of eC to reduce oxidative stress and maintain metabolic function under compound stressors (Abo Gamar et al., 2019; Zhou et al., 2020).

Transcriptomic analysis supports this hypothesis. In the eC+D and eC+eT+D treatments, we observed significant upregulation of *PEROXIDASE 5-LIKE*, which encodes an enzyme involved in ROS scavenging, particularly the reduction of hydrogen peroxide (H_2O_2) (Laxa et al., 2019). Drought and heat often trigger excessive ROS accumulation, and eC may help maintain redox homeostasis by activating specific peroxidase isoforms required for ROS detoxification under these stress conditions (AbdElgawad et al., 2023). Under eT+D, GO enrichment analysis further identified pathway associated with photosynthesis-antenna proteins, correlating with significant upregulation of *LCHB* (Wang et al., 2017).

In addition, we observed enrichment of pathways related to protein processing in the endoplasmic reticulum (ER), highlighting its role in thermotolerance through the unfolded protein response (UPR). This pathway encompasses key components of the UPR, a mechanism that restores ER homeostasis by enhancing the protein-folding capacity and facilitating the degradation of misfolded proteins under heat-induced stress (Park and Park, 2019; Pastor-Cantizano et al., 2020). Notably, these ER-related pathways were enriched in all treatments (single or combined) containing eT or D, indicating that ER-based stress responses may represent a common adaptive strategy across different combined stress scenarios (Howell, 2013).

The three-factor treatment also upregulated *GLUTATHIONE S-TRANSFERASE 1 (GSTF1)*, an enzyme that plays a significant role in responses to abiotic stress (Kumar et al., 2018; Foyer and Noctor, 2005). *GSTF1* may contribute, by conjugating glutathione, to detoxifying harmful oxidative compounds, thereby supporting cellular protection against oxidative stress associated with ROS (Gao et al., 2022). Beyond detoxification, GSTs also contribute to plant growth, development, and secondary metabolism (Lin et al., 2025). Additionally, GO-terms enrichment analysis identified pathways involved in plant abiotic stress responses, such as sugar metabolism. Acting as both energy sources and signalling molecules, increased soluble sugar concentrations may protect plants from stress-induced damage (Zinta et al., 2018). Among other mechanisms, sugars can act as osmoprotectants, helping plants maintain cell hydration during dehydration caused by drought or other abiotic stressors (Padhan et al., 2020).

We also observed the significant enrichment of TF families such as bHLH, bZIP, and WRKY under combined treatments, reflecting their central functions in regulating downstream protective mechanisms (Qin et al., 2008; Ye et al., 2021; Yu et al., 2023; Agarwal et al., 2019; Chander et al., 2018). For example, WRKY TFs are involved in signalling pathways mediated by stress-related phytohormones such as ABA and SA (salicylic acid) (Li et al., 2020), and also participate in developmental processes including plant senescence (Wang et al., 2023). These findings are consistent with the emerging view that specific TF networks modulate plant responses to the complexity of combined stressors, and represent promising targets for enhancing crop resilience through breeding or genetic engineering approaches (Zandalinas et al., 2018).

It is important to recognise that plant responses to abiotic stressors involve complex and highly integrated gene networks and pathways. Consequently, it is unlikely that a single "silver bullet" gene could provide broad-spectrum stress tolerance on its own (Palmgren and Shabala, 2024). Instead, improving resilience will require coordinated manipulation of multiple regulatory nodes across key pathways.

Limitations and future perspectives

This study provides new insights into wheat adaptation under climate-relevant conditions, but several limitations should be noted. First, we examined a single genotype; different cultivars may display distinct morpho-physiological and transcriptomic responses to combined environmental factors. Future work should include multi-genotype comparisons to capture variation in stress resilience. Second, growth-chamber conditions do not fully reflect field complexity, where soil heterogeneity, microbiomes and fluctuating weather also shape responses. Third, transcriptomics alone cannot resolve post-transcriptional regulation or metabolic reprogramming; integrating proteomic and metabolomic data would provide a more complete view.

From a translational perspective, biased homoeologs and subgenome-specific marker genes emerging from our analyses are promising candidates for functional validation, marker development and homoeolog-aware editing. At the same time, the substantial balanced component advises caution: interventions targeting a single homoeolog may be buffered by the remaining copies. Prioritising biased triads for validation, testing for dosage effects and redundancy, and combining multi-omics with field trials will help refine targets and support the development of climate-smart cultivars with stable performance under future environments.

Declaration of generative AI and AI-assisted technologies in the writing process

During the preparation of this work, the authors used chatGPT to correct English grammar and refine scientific style without changing text content. After using this tool/service, the authors reviewed and edited the content as needed and take full responsibility for the content of the publication.

CRediT authorship contribution statement

Zbyněk Milec: Writing – original draft, Visualization, Formal analysis. **Kashif Nawaz:** Formal analysis, Data curation. **Swati Puranik:**

Formal analysis. **Anna Nowicka:** Writing – original draft, Formal analysis. **Martin Kovačik:** Formal analysis, Data curation. **Hana Findurová:** Formal analysis. **Emmanuel Opoku:** Formal analysis. **Ales Pecinka:** Writing – review & editing. **Karel Klem:** Writing – review & editing, Conceptualization. **Otmar Urban:** Writing – review & editing, Conceptualization. **Pranav Pankaj Sahu:** Writing – review & editing, Supervision, Project administration, Funding acquisition, Conceptualization.

Declaration of competing interest

The authors declare that they have no known competing financial interests or personal relationships that could have appeared to influence the work reported in this paper.

Acknowledgments

This research was funded by the Czech Science Foundation (Grant No. 20–25845Y) awarded to PPS. ZM, KK and OU were supported by the Ministry of Education, Youth and Sports of the Czech Republic - AdAgriF project (CZ.02.01.01/00/22_008/0004635) and CzeCOS project (LM2023048), and by the Ministry of Agriculture of the Czech Republic - NAZV (QK23020080) AN, MK and AP were supported by the project Towards Next Generation Crops (reg. no. CZ.02.01.01/00/22_008/0004581) of the ERDF Programme Johannes Amos Comenius.

Supplementary materials

Supplementary material associated with this article can be found, in the online version, at doi:10.1016/j.stress.2025.101115.

Data availability

RNA sequencing data were deposited at the Gene Expression Omnibus (GEO; https://www.ncbi.nlm.nih.gov/geo/) with assigned accession number GSE294406. All other relevant data can be found within the manuscript and its supporting materials.

References

AbdElgawad, H., Zinta, G., Hornbacher, J., Papenbrock, J., Markakis, M.N., Asard, H., Beemster, G.T.S., 2023. Elevated CO2 mitigates the impact of drought stress by upregulating glucosinolate metabolism in Arabidopsis thaliana. Plant Cell Environ. 46, 812–830. https://doi.org/10.1111/pce.14521.

Abdelhakim, L.O.A., Palma, C.F.F., Zhou, R., Wollenweber, B., Ottosen, C.-O., Rosenqvist, E., 2021. The effect of individual and combined drought and heat stress under elevated CO2 on physiological responses in spring wheat genotypes. Plant Physiol. Biochem. 162, 301–314. https://doi.org/10.1016/j.plaphy.2021.02.015.

Abo Gamar, M.I., Kisiala, A., Emery, R.J.N., Yeung, E.C., Stone, S.L., Qaderi, M.M., 2019. Elevated carbon dioxide decreases the adverse effects of higher temperature and drought stress by mitigating oxidative stress and improving water status in Arabidopsis thaliana. Planta 250, 1191–1214. https://doi.org/10.1007/s00425-019-03213-3.

Agarwal, P., Baranwal, V.K., Khurana, P., 2019. Genome-wide analysis of bZIP transcription factors in wheat and functional characterization of a TabZIP under abiotic stress. Sci. Rep. 9, 4608. https://doi.org/10.1038/s41598-019-40659-7.

Ainsworth, E.A., Long, S.P., 2005. What have we learned from 15 years of free-air CO2 enrichment (FACE)? A meta-analytic review of the responses of photosynthesis, canopy properties and plant production to rising CO2. New Phytol. 165, 351–372. https://doi.org/10.1111/j.1469-8137.2004.01224.x.

Atkinson, N.J., Urwin, P.E., 2012. The interaction of plant biotic and abiotic stresses: from genes to the field. J. Exp. Bot. 63, 3523–3543. https://doi.org/10.1093/jxb/ers100.

Avila, R.T., Cardoso, A.A., De Almeida, W.L., Costa, L.C., Machado, K.L.G., Barbosa, M.L., De Souza, R.P.B., Oliveira, L.A., Batista, D.S., Martins, S.C.V., Ramalho, J.D.C., DaMatta, F.M., 2020. Coffee plants respond to drought and elevated [CO2] through changes in stomatal function, plant hydraulic conductance, and aquaporin expression. Environ. Exp. Bot. 177, 104148. https://doi.org/10.1016/j.envexpbot.2020.104148.

Azameti, M.K., Ranjan, A., Singh, P.K., Gaikwad, K., Singh, A.K., Dalal, M., Arora, A., Rai, V., Padaria, J.C., 2022. Transcriptome profiling reveals the genes and pathways involved in thermo-tolerance in wheat (Triticum aestivum L.) genotype Raj 3765. Sci. Rep. 12, 14831. https://doi.org/10.1038/s41598-022-18625-7.

Bach, L., Gojon, A., 2023. Root system growth and development responses to elevated CO2: underlying signalling mechanisms and role in improving plant CO2 capture and soil C storage. Biochem. J. 480, 753–771. https://doi.org/10.1042/BCJ20220245.

Bita, C., Gerats, T., 2013. Plant tolerance to high temperature in a changing environment: scientific fundamentals and production of heat stress-tolerant crops. Front. Plant Sci. 4. https://doi.org/10.3389/fpls.2013.00273.

Borrill, P., Ramirez-Gonzalez, R., Uauy, C., 2016. expVIP: a customizable RNA-seq data analysis and visualization platform. Plant Physiol. 170, 2172–2186. https://doi.org/10.1104/pp.15.01667.

Cao, Q., Li, G., Liu, F., 2022. Elevated CO2 enhanced water use efficiency of wheat to progressive drought stress but not on maize. Front. Plant Sci. 13. https://doi.org/10.3389/fpls.2022.953712.

Chander, S., Almeida, D.M., Serra, T.S., Jardim-Messeder, D., Barros, P.M., Lourenço, T. F., Figueiredo, D.D., Margis-Pinheiro, M., Costa, J.M., Oliveira, M.M., Saibo, N.J.M., 2018. *OsICE1* transcription factor improves photosynthetic performance and reduces grain losses in rice plants subjected to drought. Environ. Exp. Bot. 150, 88–98. https://doi.org/10.1016/j.envexpbot.2018.02.004.

Chavan, S.G., Duursma, R.A., Tausz, M., Ghannoum, O., 2019. Elevated CO2 alleviates the negative impact of heat stress on wheat physiology but not on grain yield. J. Exp. Bot. 70, 6447–6459. https://doi.org/10.1093/jxb/erz386.

Chen, J.-H., Jiang, H.-W., Hsieh, E.-J., Chen, H.-Y., Chien, C.-T., Hsieh, H.-L., Lin, T.-P., 2012. Drought and salt stress tolerance of an arabidopsis glutathione S-transferase U17 knockout mutant are attributed to the combined effect of glutathione and Abscisic Acid1[C][W][OA]. Plant Physiol. 158, 340–351. https://doi.org/10.1104/pp.111.181875.

Cohen, I., Zandalinas, S.I., Huck, C., Fritschi, F.B., Mittler, R., 2021. Meta-analysis of drought and heat stress combination impact on crop yield and yield components. Physiol. Plant 171, 66–76. https://doi.org/10.1111/ppl.13203.

Cominelli, E., Galbiati, M., Vavasseur, A., Conti, L., Sala, T., Vuylsteke, M., Leonhardt, N., Dellaporta, S.L., Tonelli, C., 2005. A guard-cell-specific MYB transcription factor regulates stomatal movements and plant drought tolerance. Curr. Biol. 15, 1196–1200. https://doi.org/10.1016/j.cub.2005.05.048.

Concia, L., Veluchamy, A., Ramirez-Prado, J.S., Martin-Ramirez, A., Huang, Y., Perez, M., Domenichini, S., Rodriguez Granados, N.Y., Kim, S., Blein, T., Duncan, S., Pichot, C., Manza-Mianza, D., Juery, C., Paux, E., Moore, G., Hirt, H., Bergounioux, C., Crespi, M., Mahfouz, M.M., Bendahmane, A., Liu, C., Hall, A., Raynaud, C., Latrasse, D., Benhamed, M., 2020. Wheat chromatin architecture is organized in genome territories and transcription factories. Genome Biol. 21, 104. https://doi.org/10.1186/s13059-020-01998-1.

Erenstein, O., Jaleta, M., Mottaleb, K.A., Sonder, K., Donovan, J., Braun, H.-J., 2022. Global trends in wheat production, consumption and trade. In: Reynolds, M.P., Braun, H.-J. (Eds.), Wheat Improvement: Food Security in a Changing Climate. Springer International Publishing, Cham, pp. 47–66. https://doi.org/10.1007/978-3-030-90673-3_4.

Foyer, C.H., Noctor, G., 2005. Redox homeostasis and antioxidant signaling: a metabolic interface between stress perception and physiological responses. Plant Cell 17, 1866–1875. https://doi.org/10.1105/tpc.105.033589.

Gao, H., Yu, C., Liu, R., Li, X., Huang, H., Wang, X., Zhang, C., Jiang, N., Li, X., Cheng, S., Zhang, H., Li, B., 2022. The glutathione S-transferase PtGSTF1 improves biomass production and salt tolerance through regulating xylem cell proliferation, ion homeostasis and reactive oxygen species scavenging in Poplar. Int. J. Mol. Sci. 23, 11288. https://doi.org/10.3390/ijms231911288.

Grondin, A., Rodrigues, O., Verdoucq, L., Merlot, S., Leonhardt, N., Maurel, C., 2015. Aquaporins contribute to ABA-triggered stomatal closure through OST1-mediated phosphorylation. Plant Cell 27, 1945–1954. https://doi.org/10.1105/tpc.15.00421.

Hamilton, N.E., Ferry, M., 2018. **ggtern** : ternary diagrams using ggplot2. J. Stat. Soft. 87. https://doi.org/10.18637/jss.v087.c03.

He, Y., Zhou, K., Wu, Z., Li, B., Fu, J., Lin, C., Jiang, D., 2019. Highly efficient nanoscale analysis of plant stomata and cell surface using polyaddition silicone rubber. Front. Plant Sci. 10. https://doi.org/10.3389/fpls.2019.01569.

Holman, I.P., Hess, T.M., Rey, D., Knox, J.W., 2021. A multi-level framework for adaptation to drought within temperate agriculture. Front. Environ. Sci. 8. https://doi.org/10.3389/fenvs.2020.589871.

Howell, S.H., 2013. Endoplasmic reticulum stress responses in plants. Annu Rev. Plant Biol. 64, 477–499. https://doi.org/10.1146/annurev-arplant-050312-120053.

Huang, D.W., Sherman, B.T., Lempicki, R.A., 2009. Systematic and integrative analysis of large gene lists using DAVID bioinformatics resources. Nat. Protoc. 4, 44–57. https://doi.org/10.1038/nprot.2008.211.

Jung, C., Seo, J.S., Han, S.W., Koo, Y.J., Kim, C.H., Song, S.I., Nahm, B.H., Choi, Y.D., Cheong, J.-J., 2008. Overexpression of AtMYB44 enhances stomatal closure to confer abiotic stress tolerance in transgenic arabidopsis. Plant Physiol. 146, 623–635. https://doi.org/10.1104/pp.107.110981.

Kan, Y., Mu, X.-R., Gao, J., Lin, H.-X., Lin, Y., 2023. The molecular basis of heat stress responses in plants. Mol. Plant 16, 1612–1634. https://doi.org/10.1016/j.molp.2023.09.013.

Khaliq, I., Irshad, A., Ahsan, M., 2008. Awns and flag leaf contribution towards grain yield in spring wheat (Triticum aestivum L.). Cereal. Res. Commun. 36, 65–76. https://doi.org/10.1556/CRC.36.2008.1.7.

Kim, D., Paggi, J.M., Park, C., Bennett, C., Salzberg, S.L., 2019. Graph-based genome alignment and genotyping with HISAT2 and HISAT-genotype. Nat. Biotechnol. 37, 907–915. https://doi.org/10.1038/s41587-019-0201-4.

Kumar, S., Trivedi, P.K., Glutathione, S-Transferases, 2018. Role in combating abiotic stresses including arsenic detoxification in plants. Front. Plant Sci. 9. https://doi.org/10.3389/fpls.2018.00751.

Langfelder, P., Horvath, S., 2008. WGCNA: an R package for weighted correlation network analysis. BMC. Bioinform. 9, 559. https://doi.org/10.1186/1471-2105-9-559.

Laxa, M., Liebthal, M., Telman, W., Chibani, K., Dietz, K.-J., 2019. The role of the plant antioxidant system in drought tolerance. Antioxidants 8, 94. https://doi.org/10.3390/antiox8040094.

Li, W., Pang, S., Lu, Z., Jin, B., 2020. Function and mechanism of WRKY transcription factors in abiotic stress responses of plants. Plants 9, 1515. https://doi.org/10.3390/plants9111515.

Lin, C., Zhang, Z., Zhang, Z., Long, Y., Shen, X., Zhang, J., Wang, Y., 2025. The role of glutathione S-transferase in the regulation of plant growth, and responses to environmental stresses. Phyton. (B Aires) 94, 583–601. https://doi.org/10.32604/phyton.2025.063086.

Lin, Y., Shen, C., Lin, E., Hao, X., Han, X., 2016. Transcriptome response of wheat Norin 10 to long-term elevated CO2 under high yield field condition. J. Integr. Agric. 15, 2142–2152. https://doi.org/10.1016/S2095-3119(16)61421-1.

Liu, Z., Xin, M., Qin, J., Peng, H., Ni, Z., Yao, Y., Sun, Q., 2015. Temporal transcriptome profiling reveals expression partitioning of homeologous genes contributing to heat and drought acclimation in wheat (Triticum aestivum L.). BMC. Plant Biol. 15, 152. https://doi.org/10.1186/s12870-015-0511-8.

Long, S.P., Ainsworth, E.A., Leakey, A.D.B., Nösberger, J., Ort, D.R., 2006. Food for thought: lower-than-expected crop yield stimulation with rising CO2 concentrations. Science (1979) 312, 1918–1921. https://doi.org/10.1126/science.1114722.

Lorite, I.J., Castilla, A., Cabezas, J.M., Alza, J., Santos, C., Porras, R., Gabaldón-Leal, C., Muñoz-Marchal, E., Sillero, J.C., 2023. Analyzing the impact of extreme heat events and drought on wheat yield and protein concentration, and adaptation strategies using long-term cultivar trials under semi-arid conditions. Agric. For. Meteorol. 329, 109279. https://doi.org/10.1016/j.agrformet.2022.109279.

Love, M.I., Huber, W., Anders, S., 2014. Moderated estimation of fold change and dispersion for RNA-seq data with DESeq2. Genome Biol. 15, 550. https://doi.org/10.1186/s13059-014-0550-8.

Ma, J., Li, R., Wang, H., Li, D., Wang, X., Zhang, Y., Zhen, W., Duan, H., Yan, G., Li, Y., 2017. Transcriptomics analyses reveal wheat responses to drought stress during reproductive stages under field conditions. Front. Plant Sci. 8. https://doi.org/10.3389/fpls.2017.00592.

Mahmood, A., Alam, K., Salam, A., Iqbal, S., 1991. Effect of flag leaf removal on grain yield, its components and quality of hexaploid wheat. Cereal. Res. Commun. 19, 305–310.

Maurel, C., Verdoucq, L., Rodrigues, O., 2016. Aquaporins and plant transpiration. Plant Cell Environ. 39, 2580–2587. https://doi.org/10.1111/pce.12814.

Meng, J., Guo, J., Li, T., Chen, Z., Li, M., Zhao, D., Tao, J., 2022. Analysis and functional verification of PlPM19L gene associated with drought-resistance in paeonia lactiflora pall. Int. J. Mol. Sci. 23, 15695. https://doi.org/10.3390/ijms232415695.

Merilo, E., Jõesaar, I., Brosché, M., Kollist, H., 2014. To open or to close: species-specific stomatal responses to simultaneously applied opposing environmental factors. New Phytol. 202, 499–508. https://doi.org/10.1111/nph.12667.

Miloro, F., Kis, A., Havelda, Z., Dalmadi, Á., 2024. Barley AGO4 proteins show overlapping functionality with distinct small RNA-binding properties in heterologous complementation. Plant Cell Rep. 43, 96. https://doi.org/10.1007/s00299-024-03177-z.

O'Leary, G.J., Christy, B., Nuttall, J., Huth, N., Cammarano, D., Stöckle, C., Basso, B., Shcherbak, I., Fitzgerald, G., Luo, Q., Farre-Codina, I., Palta, J., Asseng, S., 2015. Response of wheat growth, grain yield and water use to elevated CO2 under a free-air CO2 enrichment (FACE) experiment and modelling in a semi-arid environment. Glob. Chang. Biol. 21, 2670–2686. https://doi.org/10.1111/gcb.12830.

Ohama, N., Sato, H., Shinozaki, K., Yamaguchi-Shinozaki, K., 2017. Transcriptional regulatory network of plant heat stress response. Trends. Plant Sci. 22, 53–65. https://doi.org/10.1016/j.tplants.2016.08.015.

Onyemaobi, O., Sangma, H., Garg, G., Wallace, X., Kleven, S., Suwanchaikasem, P., Roessner, U., Dolferus, R., 2021. Reproductive stage drought tolerance in wheat: importance of stomatal conductance and plant growth regulators. Genes. (Basel) 12, 1742. https://doi.org/10.3390/genes12111742.

Intergovernmental Panel on Climate Change, 2015. In: Pachauri, R.K., Mayer, L. (Eds.), Climate Change 2014: Synthesis report, Intergovernmental Panel On Climate Change. Geneva, Switzerland.

Padhan, B.K., Sathee, L., Meena, H.S., Adavi, S.B., Jha, S.K., Chinnusamy, V., 2020. CO2 Elevation accelerates phenology and alters carbon/nitrogen metabolism vis-à-vis ROS abundance in bread wheat. Front. Plant Sci. 11, 1061. https://doi.org/10.3389/fpls.2020.01061.

Palmgren, M., Shabala, S., 2024. Adapting crops for climate change: regaining lost abiotic stress tolerance in crops. Front. Sci. 2. https://doi.org/10.3389/fsci.2024.1416023.

Park, C.-J., Park, J.M., 2019. Endoplasmic reticulum plays a critical role in integrating signals generated by both biotic and abiotic stress in plants. Front. Plant Sci. 10. https://doi.org/10.3389/fpls.2019.00399.

Pastor-Cantizano, N., Ko, D.K., Angelos, E., Pu, Y., Brandizzi, F., 2020. Functional diversification of ER stress responses in Arabidopsis. Trends. Biochem. Sci. 45, 123–136. https://doi.org/10.1016/j.tibs.2019.10.008.

Pflüger, T., Jensen, S.M., Liu, F., Rosenqvist, E., 2024. Leaf gas exchange responses to combined heat and drought stress in wheat genotypes with varied stomatal density. Environ. Exp. Bot. 228, 105984. https://doi.org/10.1016/j.envexpbot.2024.105984.

Pietrzykowska, M., Suorsa, M., Semchonok, D.A., Tikkanen, M., Boekema, E.J., Aro, E.-M., Jansson, S., 2014. The light-harvesting chlorophyll a/b binding proteins Lhcb1 and Lhcb2 play complementary roles during State transitions in Arabidopsis[C][W][OPEN]. Plant Cell 26, 3646–3660. https://doi.org/10.1105/tpc.114.127373.

Prasad, P.V.V., Pisipati, S.R., Momčilović, I., Ristic, Z., 2011. Independent and combined effects of high temperature and drought stress during grain filling on plant yield and chloroplast EF-tu expression in spring wheat. J. Agron. Crop. Sci. 197, 430–441. https://doi.org/10.1111/j.1439-037X.2011.00477.x.

Qin, D., Wu, H., Peng, H., Yao, Y., Ni, Z., Li, Z., Zhou, C., Sun, Q., 2008. Heat stress-responsive transcriptome analysis in heat susceptible and tolerant wheat (Triticum aestivum L.) by using Wheat Genome Array. BMC. Genomics. 9, 432. https://doi.org/10.1186/1471-2164-9-432.

Ramírez-González, R.H., Borrill, P., Lang, D., Harrington, S.A., Brinton, J., Venturini, L., Davey, M., Jacobs, J., van Ex, F., Pasha, A., Khedikar, Y., Robinson, S.J., Cory, A.T., Florio, T., Concia, L., Juery, C., Schoonbeek, H., Steuernagel, B., Xiang, D., Ridout, C. J., Chalhoub, B., Mayer, K.F.X., Benhamed, M., Latrasse, D., Bendahmane, A., Consortium, International Wheat Genome Sequencing, Wulff, B.B.H., Appels, R., Tiwari, V., Datla, R., Choulet, F., Pozniak, C.J., Provart, N.J., Sharpe, A.G., Paux, E., Spannagl, M., Bräutigam, A., Uauy, C., 2018. The transcriptional landscape of polyploid wheat. Science (1979) 361, eaar6089. https://doi.org/10.1126/science.aar6089.

Ravi, B., Foyer, C.H., Pandey, G.K., 2023. The integration of reactive oxygen species (ROS) and calcium signalling in abiotic stress responses. Plant Cell Environ. 46, 1985–2006. https://doi.org/10.1111/pce.14596.

Rerksiri, W., Zhang, X., Xiong, H., Chen, X., 2013. Expression and promoter analysis of six heat stress-inducible genes in rice. The Sci. World J. 2013, 397401. https://doi.org/10.1155/2013/397401.

Reynolds, M.P., Lewis, J.M., Ammar, K., Basnet, B.R., Crespo-Herrera, L., Crossa, J., Dhugga, K.S., Dreisigacker, S., Juliana, P., Karwat, H., Kishii, M., Krause, M.R., Langridge, P., Lashkari, A., Mondal, S., Payne, T., Pequeno, D., Pinto, F., Sansaloni, C., Schulthess, U., Singh, R.P., Sonder, K., Sukumaran, S., Xiong, W., Braun, H.J., 2021. Harnessing translational research in wheat for climate resilience. J. Exp. Bot. 72, 5134–5157. https://doi.org/10.1093/jxb/erab256.

Rizhsky, L., Liang, H., Mittler, R., 2002. The combined effect of drought stress and heat shock on gene expression in tobacco. Plant Physiol. 130, 1143–1151. https://doi.org/10.1104/pp.006858.

Rodrigues, O., Reshetnyak, G., Grondin, A., Saijo, Y., Leonhardt, N., Maurel, C., Verdoucq, L., 2017. Aquaporins facilitate hydrogen peroxide entry into guard cells to mediate ABA- and pathogen-triggered stomatal closure. Proc. Natl. Acad. Sci. 114, 9200–9205. https://doi.org/10.1073/pnas.1704754114.

Sade, N., Gebretsadik, M., Seligmann, R., Schwartz, A., Wallach, R., Moshelion, M., 2010. The role of tobacco Aquaporin1 in improving water use efficiency, hydraulic conductivity, and yield production under salt stress. Plant Physiol. 152, 245–254. https://doi.org/10.1104/pp.109.145854.

Sato, H., Mizoi, J., Shinozaki, K., Yamaguchi-Shinozaki, K., 2024. Complex plant responses to drought and heat stress under climate change. The Plant J. 117, 1873–1892. https://doi.org/10.1111/tpj.16612.

Shaar-Moshe, L., Blumwald, E., Peleg, Z., 2017. Unique physiological and transcriptional shifts under combinations of salinity, drought, and heat. Plant Physiol. 174, 421–434. https://doi.org/10.1104/pp.17.00030.

Shah, M.M., Gill, K.S., Baenziger, P.S., Yen, Y., Kaeppler, S.M., Ariyarathne, H.M., 1999. Molecular mapping of loci for agronomic traits on chromosome 3A of bread wheat. Crop. Sci. 39, 1728. https://doi.org/10.2135/cropsci1999.3961728x.

Shanmugam, S., Kjaer, K.H., Ottosen, C.-O., Rosenqvist, E., Kumari Sharma, D., Wollenweber, B., 2013. The alleviating effect of elevated CO2 on heat stress susceptibility of two wheat (riticum aestivum L.) cultivars. J. Agron. Crop. Sci. 199, 340–350. https://doi.org/10.1111/jac.12023.

Sherman, B.T., Hao, M., Qiu, J., Jiao, X., Baseler, M.W., Lane, H.C., Imamichi, T., Chang, W., 2022. DAVID: a web server for functional enrichment analysis and functional annotation of gene lists (2021 update). Nucleic. Acids. Res. 50, W216–W221. https://doi.org/10.1093/nar/gkac194.

Shiferaw, B., Smale, M., Braun, H.-J., Duveiller, E., Reynolds, M., Muricho, G., 2013. Crops that feed the world 10. Past successes and future challenges to the role played by wheat in global food security. Food Sec. 5, 291–317. https://doi.org/10.1007/s12571-013-0263-y.

Su, P., Yan, J., Li, W., Wang, L., Zhao, J., Ma, X., Li, A., Wang, H., Kong, L., 2020. A member of wheat class III peroxidase gene family, TaPRX-2A, enhanced the tolerance of salt stress. BMC. Plant Biol. 20, 392. https://doi.org/10.1186/s12870-020-02602-1.

Suzuki, N., Rivero, R.M., Shulaev, V., Blumwald, E., Mittler, R., 2014. Abiotic and biotic stress combinations. New Phytol. 203, 32–43. https://doi.org/10.1111/nph.12797.

Tahmasebi, S., Heidari, B., Pakniyat, H., McIntyre, C.L., 2017. Mapping QTLs associated with agronomic and physiological traits under terminal drought and heat stress conditions in wheat (Triticum aestivum L.). Genome 60, 26–45. https://doi.org/10.1139/gen-2016-0017.

Tricker, P.J., ElHabti, A., Schmidt, J., Fleury, D., 2018. The physiological and genetic basis of combined drought and heat tolerance in wheat. J. Exp. Bot. 69, 3195–3210. https://doi.org/10.1093/jxb/ery081.

Tripathy, K.P., Mukherjee, S., Mishra, A.K., Mann, M.E., Williams, A.P., 2023. Climate change will accelerate the high-end risk of compound drought and heatwave events. Proc. Natl. Acad. Sci. 120, e2219825120. https://doi.org/10.1073/pnas.2219825120.

van der Kooi, C.J., Reich, M., Löw, M., De Kok, L.J., Tausz, M., 2016. Growth and yield stimulation under elevated CO2 and drought: a meta-analysis on crops. Environ. Exp. Bot. 122, 150–157. https://doi.org/10.1016/j.envexpbot.2015.10.004.

Vanaja, M., Sarkar, B., Sathish, P., Jyothi Lakshmi, N., Yadav, S.K., Mohan, C., Sushma, A., Yashavanth, B.S., Srinivasa Rao, M., Prabhakar, M., Singh, V.K., 2024. Elevated CO2 ameliorates the high temperature stress effects on physio-biochemical, growth, yield traits of maize hybrids. Sci. Rep. 14, 2928. https://doi.org/10.1038/s41598-024-53343-2.

Vicente, R., Bolger, A.M., Martínez-Carrasco, R., Pérez, P., Gutiérrez, E., Usadel, B., Morcuende, R., 2019. De novo transcriptome analysis of durum wheat flag leaves provides new insights into the regulatory response to elevated CO2 and high temperature. Front. Plant Sci. 10. https://doi.org/10.3389/fpls.2019.01605.

Wang, H., Chen, W., Xu, Z., Chen, M., Yu, D., 2023a. Functions of WRKYs in plant growth and development. Trends. Plant Sci. 28, 630–645. https://doi.org/10.1016/j.tplants.2022.12.012.

Wang, K., Liu, Y., Tian, J., Huang, K., Shi, T., Dai, X., Zhang, W., 2017. Transcriptional profiling and identification of heat-responsive genes in perennial ryegrass by RNA-sequencing. Front. Plant Sci. 8, 1032. https://doi.org/10.3389/fpls.2017.01032.

Wang, L., Wei, J., Shi, X., Qian, W., Mehmood, J., Yin, Y., Jia, H., 2023b. Identification of the light-harvesting chlorophyll a/b binding protein gene Family in peach (Prunus persica L.) and their expression under drought stress. Genes. (Basel) 14, 1475. https://doi.org/10.3390/genes14071475.

Wang, X., Liu, Y., Zhao, P., Hou, W., Cheng, M., Shi, X., Simmonds, J., Borrill, P., Wang, X., Ji, W., Xu, S., 2025. HebQTLs reveal intra-subgenome regulation inducing unbalanced expression and function among bread wheat homoeologs. Genome Biol. 26, 218. https://doi.org/10.1186/s13059-025-03694-4.

Wang, Z., Wang, C., Liu, S., 2022. Elevated CO2 alleviates adverse effects of drought on plant water relations and photosynthesis: a global meta-analysis. J. Ecol. 110, 2836–2849. https://doi.org/10.1111/1365-2745.13988.

Xiong, W., Reynolds, M.P., Montes, C., Crossa, J., Snapp, S., Akin, B., Mesut, K., Ozdemir, F., Li, H., He, Z., Wang, D., Chen, F., 2024. New wheat breeding paradigms for a warming climate. Nat. Clim. Chang. 14, 869–875. https://doi.org/10.1038/s41558-024-02069-0.

Xu, F., Wang, K., Yuan, W., Xu, W., Liu, S., Kronzucker, H.J., Chen, G., Miao, R., Zhang, M., Ding, M., Xiao, L., Kai, L., Zhang, J., Zhu, Y., 2019. Overexpression of rice aquaporin OsPIP1;2 improves yield by enhancing mesophyll CO2 conductance and phloem sucrose transport. J. Exp. Bot. 70, 671–681. https://doi.org/10.1093/jxb/ery386.

Xu, Y.-H., Liu, R., Yan, L., Liu, Z.-Q., Jiang, S.-C., Shen, Y.-Y., Wang, X.-F., Zhang, D.-P., 2012. Light-harvesting chlorophyll a/b-binding proteins are required for stomatal response to abscisic acid in Arabidopsis. J. Exp. Bot. 63, 1095–1106. https://doi.org/10.1093/jxb/err315.

Yang, D.-H., Paulsen, H., Andersson, B., 2000. The N-terminal domain of the light-harvesting chlorophyll *a/b*-binding protein complex (LHCII) is essential for its acclimative proteolysis. FEBS Lett. 466, 385–388. https://doi.org/10.1016/S0014-5793(00)01107-8.

Yao, L., Cheng, X., Gu, Z., Huang, W., Li, S., Wang, L., Wang, Y.-F., Xu, P., Ma, H., Ge, X., 2018. The AWPM-19 Family protein OsPM1 mediates abscisic acid influx and drought response in rice. Plant Cell 30, 1258–1276. https://doi.org/10.1105/tpc.17.00770.

Ye, H., Qiao, L., Guo, H., Guo, L., Ren, F., Bai, J., Wang, Y., 2021. Genome-wide identification of wheat WRKY gene Family reveals that TaWRKY75-A is referred to drought and salt resistances. Front. Plant Sci. 12. https://doi.org/10.3389/fpls.2021.663118.

Yu, Y., Song, T., Wang, Y., Zhang, M., Li, N., Yu, M., Zhang, S., Zhou, H., Guo, S., Bu, Y., Wang, T., Xiang, J., Zhang, X., 2023. The wheat WRKY transcription factor TaWRKY1-2D confers drought resistance in transgenic *arabidopsis* and wheat (*Triticum aestivum* L.). Int. J. Biol. Macromol. 226, 1203–1217. https://doi.org/10.1016/j.ijbiomac.2022.11.234.

Zandalinas, S.I., Mittler, R., 2022. Plant responses to multifactorial stress combination. New Phytol. 234, 1161–1167. https://doi.org/10.1111/nph.18087.

Zandalinas, S.I., Mittler, R., Balfagón, D., Arbona, V., Gómez-Cadenas, A., 2018. Plant adaptations to the combination of drought and high temperatures. Physiol. Plant 162, 2–12. https://doi.org/10.1111/ppl.12540.

Zhang, J., Wen, W., Li, H., Lu, Q., Xu, B., Huang, B., 2020a. Overexpression of an aquaporin gene PvPIP2;9 improved biomass yield, protein content, drought tolerance and water use efficiency in switchgrass (Panicum virgatum L.). GCB Bioenergy 12, 979–991. https://doi.org/10.1111/gcbb.12751.

Zhang, L., Takahashi, Y., Hsu, P.-K., Kollist, H., Merilo, E., Krysan, P.J., Schroeder, J.I., 2020b. FRET kinase sensor development reveals SnRK2/OST1 activation by ABA but not by MeJA and high CO2 during stomatal closure. Elife 9, e56351. https://doi.org/10.7554/eLife.56351.

Zhou, R., Yu, X., Wen, J., Jensen, N.B., dos Santos, T.M., Wu, Z., Rosenqvist, E., Ottosen, C.-O., 2020. Interactive effects of elevated CO2 concentration and combined heat and drought stress on tomato photosynthesis. BMC. Plant Biol. 20, 260. https://doi.org/10.1186/s12870-020-02457-6.

Zhu, F., Paul, P., Hussain, W., Wallman, K., Dhatt, B.K., Sandhu, J., Irvin, L., Morota, G., Yu, H., Walia, H., 2021. SeedExtractor: an open-source GUI for seed image analysis. Front. Plant Sci. 11. https://doi.org/10.3389/fpls.2020.581546.

Zinta, G., AbdElgawad, H., Domagalska, M.A., Vergauwen, L., Knapen, D., Nijs, I., Janssens, I.A., Beemster, G.T.S., Asard, H., 2014. Physiological, biochemical, and genome-wide transcriptional analysis reveals that elevated CO2 mitigates the impact of combined heat wave and drought stress in Arabidopsis thaliana at multiple organizational levels. Glob. Chang. Biol. 20, 3670–3685. https://doi.org/10.1111/gcb.12626.

Zinta, G., AbdElgawad, H., Peshev, D., Weedon, J.T., Van den Ende, W., Nijs, I., Janssens, I.A., Beemster, G.T.S., Asard, H., 2018. Dynamics of metabolic responses to periods of combined heat and drought in Arabidopsis thaliana under ambient and elevated atmospheric CO2. J. Exp. Bot. 69, 2159–2170. https://doi.org/10.1093/jxb/ery055.